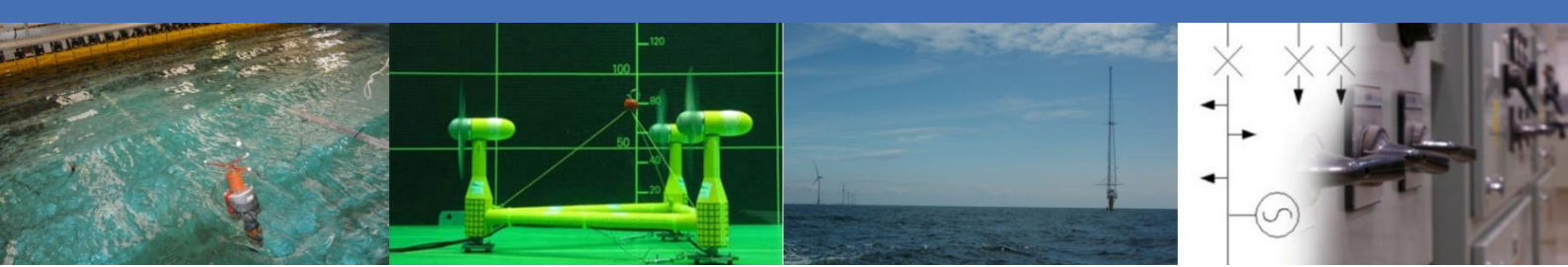




Marine Renewables Infrastructure Network



## D2.12 Collation of Wave Simulation Methods

Brendan GUILLOUZOUIC

Status: Final version  
Date: 28/01/2014



*EC FP7 "Capacities" Specific Programme  
Research Infrastructure Action*



## ABOUT MARINET















MARINET (Marine Renewables Infrastructure Network for emerging Energy Technologies) is an EC-funded network of research centres and organisations that are working together to accelerate the development of marine renewable energy - wave, tidal & offshore-wind. The initiative is funded through the EC's Seventh Framework Programme (FP7) and runs for four years until 2015. The network of 29 partners with 42 specialist marine research facilities is spread across 11 EU countries and 1 International Cooperation Partner Country (Brazil).

MARINET offers periods of free-of-charge access to test facilities at a range of world-class research centres. Companies and research groups can avail of this Transnational Access (TA) to test devices at any scale in areas such as wave energy, tidal energy, offshore-wind energy and environmental data or to conduct tests on cross-cutting areas such as power take-off systems, grid integration, materials or moorings. In total, over 700 weeks of access is available to an estimated 300 projects and 800 external users, with at least four calls for access applications over the 4-year initiative.

MARINET partners are also working to implement common standards for testing in order to streamline the development process, conducting research to improve testing capabilities across the network, providing training at various facilities in the network in order to enhance personnel expertise and organising industry networking events in order to facilitate partnerships and knowledge exchange.

The aim of the initiative is to streamline the capabilities of test infrastructures in order to enhance their impact and accelerate the commercialisation of marine renewable energy. See [www.fp7-marinet.eu](http://www.fp7-marinet.eu) for more details.

## Partners

  	<p style="text-align: center;"><b>Ireland</b></p> <p>University College Cork, HMRC (UCC_HMRC)</p> <p style="text-align: right;"><i>Coordinator</i></p> <p>Sustainable Energy Authority of Ireland (SEAI_OEDU)</p>	     	<p style="text-align: center;"><b>United Kingdom</b></p> <p>National Renewable Energy Centre Ltd. (NAREC)</p> <p>The University of Exeter (UNEXE)</p> <p>European Marine Energy Centre Ltd. (EMEC)</p> <p>University of Strathclyde (UNI_STRATH)</p> <p>The University of Edinburgh (UEDIN)</p> <p>Queen's University Belfast (QUB)</p>
	<p style="text-align: center;"><b>Denmark</b></p> <p>Aalborg Universitet (AAU)</p> <p>Danmarks Tekniske Universitet (RISOE)</p>		<p>Plymouth University(PU)</p>
 	<p style="text-align: center;"><b>France</b></p> <p>Ecole Centrale de Nantes (ECN)</p> <p>Institut Français de Recherche Pour l'Exploitation de la Mer (IFREMER)</p>	 	<p style="text-align: center;"><b>Spain</b></p> <p>Ente Vasco de la Energía (EVE)</p>

Tecnia Research & Innovation Foundation  
(TECNALIA)



**Belgium**  
1-Tech (1\_TECH)

### Netherlands

Stichting Tidal Testing Centre (TTC)



Stichting Energieonderzoek Centrum Nederland  
(ECNeth)

### Germany

Fraunhofer-Gesellschaft Zur Foerderung Der  
Angewandten Forschung E.V (Fh\_IWES)



Gottfried Wilhelm Leibniz Universität Hannover (LUH)

Universitaet Stuttgart (USTUTT)

### Portugal

Wave Energy Centre – Centro de Energia das Ondas  
(WavEC)



### Italy

Università degli Studi di Firenze (UNIFI-CRIACIV)



Università degli Studi di Firenze (UNIFI-PIN)



Università degli Studi della Tuscia (UNI\_TUS)



Consiglio Nazionale delle Ricerche (CNR-INSEAN)

### Brazil

Instituto de Pesquisas Tecnológicas do Estado de São  
Paulo S.A. (IPT)



### Norway

Sintef Energi AS (SINTEF)



Norges Teknisk-Naturvitenskapelige Universitet  
(NTNU)



## DOCUMENT INFORMATION

<b>Title</b>	Collation of wave simulations methods
<b>Distribution</b>	<b>Public</b>
<b>Document Reference</b>	MARINET-UCC-HMRC-Project acronym]
<b>User-Group Leader, Lead Author</b>	UCC-HMRC
<b>User-Group Members, Contributing Authors</b>	AAU HMRC ECN UEDIN UoP IPT IFREMER DTU QUB
<b>Infrastructure Accessed:</b>	
<b>Infrastructure Manager (or Main Contact)</b>	Judy Rea

## REVISION HISTORY

Rev.	Date	Description	Prepared by (Name)	Approved By Infrastructure	Status (Draft/Final)



				Manager	
01	11/06/2013		Brendan GUILLOUZOUIC		Draft
02	05/12/2013	Additional part on random wave simulation	Brendan GUILLOUZOUIC		Draft
0.3	28/01/2014	Sent for final review	Brendan GUILLOUZOUIC		

---

## ABOUT THIS REPORT

One of the requirements of the EC in enabling a user group to benefit from free-of-charge access to an infrastructure is that the user group must be entitled to disseminate the foreground (information and results) that they have generated under the project in order to progress the state-of-the-art of the sector. Notwithstanding this, the EC also state that dissemination activities shall be compatible with the protection of intellectual property rights, confidentiality obligations and the legitimate interests of the owner(s) of the foreground.

The aim of this report is therefore to meet the first requirement of publicly disseminating the knowledge generated through this MARINET infrastructure access project in an accessible format in order to:

- progress the state-of-the-art
- publicise resulting progress made for the technology/industry
- provide evidence of progress made along the Structured Development Plan
- provide due diligence material for potential future investment and financing
- share lessons learned
- avoid potential future replication by others
- provide opportunities for future collaboration
- etc.

In some cases, the user group may wish to protect some of this information which they deem commercially sensitive, and so may choose to present results in a normalised (non-dimensional) format or withhold certain design data – this is acceptable and allowed for in the second requirement outlined above.

## ACKNOWLEDGEMENT

The work described in this publication has received support from MARINET, a European Community - Research Infrastructure Action under the FP7 “Capacities” Specific Programme.



## **LEGAL DISCLAIMER**

The views expressed, and responsibility for the content of this publication, lie solely with the authors. The European Commission is not liable for any use that may be made of the information contained herein. This work may rely on data from sources external to the MARINET project Consortium. Members of the Consortium do not accept liability for loss or damage suffered by any third party as a result of errors or inaccuracies in such data. The information in this document is provided “as is” and no guarantee or warranty is given that the information is fit for any particular purpose. The user thereof uses the information at its sole risk and neither the European Commission nor any member of the MARINET Consortium is liable for any use that may be made of the information.

---

## EXECUTIVE SUMMARY

**This document gives an overview of the existing testing facilities dedicated to wave energy converters (WECs). It first presents the different types of wave makers and wave tanks that are commonly used. It also contains a comparative description of the wave generating methods in terms of accordance with a target wave field. Moreover, a presentation and a quality assessment of absorption methods is carried out. Finally, it focuses on special modifications to operate in wave tanks to test marine energy devices in shallow water.**



---

## CONTENTS

<b>1</b>	<b>INTRODUCTION .....</b>	<b>11</b>
<b>2</b>	<b>DIFFERENT TYPES OF WAVE MAKERS.....</b>	<b>12</b>
2.1	DIFFERENT BY THEIR ARRANGEMENT .....	12
2.1.1	<i>Frontal</i> .....	12
2.1.2	<i>Corner</i> .....	13
2.1.3	<i>Curved / circular</i> .....	15
2.2	DIFFERENT BY THEIR CONSTRUCTION .....	18
2.2.1	<i>Hinged-flap type</i> .....	18
2.2.2	<i>Piston-type</i> .....	19
2.2.3	<i>Plunging-type</i> .....	21
2.2.4	<i>Duck-type</i> .....	22
<b>3</b>	<b>SIMULTANEOUS GENERATION OF WAVE AND CURRENT .....</b>	<b>23</b>
3.1	CURRENT GENERATION AND DIRECTIONALITY.....	24
3.2	COMBINED WAVE AND CURRENT .....	26
<b>4</b>	<b>RANDOM WAVE SIMULATION .....</b>	<b>28</b>
4.1	FREQUENCY SPECTRUM .....	28
4.1.1	<i>Deterministic techniques</i> .....	28
4.1.2	<i>Non-deterministic techniques</i> .....	30
4.2	DIRECTIONAL SPECTRUM.....	31
4.2.1	<i>Double summation method</i> .....	32
4.2.2	<i>Phase locking phenomenon</i> .....	32
4.2.3	<i>Single summation method</i> .....	32
4.3	NON-LINEAR EFFECTS .....	33
<b>5</b>	<b>ON THE ACCURATE GENERATION OF A SEA-STATE ON A GIVEN AREA OF THE TANK.....</b>	<b>34</b>
5.1	THE SNAKE'S PRINCIPLE.....	34
5.1.1	<i>Basic snake's principle</i> .....	34
5.1.2	<i>Corner method Funke &amp; miles (without diffraction)</i> .....	37
5.2	ELABORATED METHODS .....	39
5.2.1	<i>Principle</i> .....	39
5.2.2	<i>Presentation of four elaborated methods</i> .....	42
5.3	GENERATION OF AN ARBITRARY WAVE-FIELD IN AN ARBITRARY BASIN (AMOEBEA) .....	49
5.3.1	<i>AMOEBEA wave generation principle</i> .....	49
5.3.2	<i>Arbitrarily configured basin</i> .....	50
5.4	LIMITATIONS IN WAVE GENERATION.....	52
5.4.1	<i>Evanescence waves</i> .....	52
5.4.2	<i>Free waves</i> .....	55

---

5.4.3	<i>Return current</i> .....	58
<b>6</b>	<b>WAVE ABSORPTION METHODS</b> .....	<b>59</b>
6.1	PASSIVE ABSORBERS (BEACHES).....	59
6.2	ACTIVE ABSORBERS .....	62
6.2.1	<i>Presentation.</i> .....	62
6.2.2	<i>Principle and equation of motion</i> .....	63
6.2.3	<i>The control system</i> .....	69
6.2.4	<i>Absorption efficiency</i> .....	74
6.2.5	<i>Frequency adaptation.</i> .....	79
<b>7</b>	<b>SHALLOW WATER ASPECTS FOR MARINE ENERGY DEVICES</b> .....	<b>81</b>
<b>8</b>	<b>CONCLUSION</b> .....	<b>82</b>
<b>9</b>	<b>REFERENCES</b> .....	<b>83</b>

---

# 1 INTRODUCTION

Physical modelling offers several benefits. It allows testing a scaled model, which reduces the construction cost of the prototype. The generation of waves in a controlled environment allows the possibility to generate waves with specific characteristics and with good repeatability. However, the use of physical models requires generating waves in basin that approach the real waves found in nature.

The present report is a collation of wave simulation methods attempting to describe first the characteristics of the different types of basins, then the methods to generate complex wave fields and to achieve spurious wave absorption, and finally to discuss of particular aspects for marine energy devices.

The information comes both from several international publications whose references are given in the last pages and from the experience feedbacks of the testing facilities of Marinet project. Several facilities have been appointed to contribute to this report. However, as few contributors effectively participated, inequalities appear in some sections as each contributor obviously gave information on the facility it knows best, i.e. its own facility. Attention is given to wave generation methods and active absorption methods.

## 2 DIFFERENT TYPES OF WAVE MAKERS

The wave generation is made through a wave board animated with a prescribed motion. The earliest method was limited to sinusoidal movements of the wave board with specified amplitude and frequency. However, it was in good agreement with the linear theory. Then, modifications on the motors gave more control over the wave board motion, and allowed the generation of 2D-irregular waves, cnoidal and solitary waves, and even directional irregular waves for segmented wave makers. Mechanical characteristics of piston-type and flap-type machines were described in *La Houille Blanche* by Biésel & Suquet (1954).

### 2.1 DIFFERENT BY THEIR ARRANGEMENT

#### 2.1.1 Frontal

The frontal wave maker is the type of wave maker present in most of the facilities. The wave maker is composed of several elements (pistons, flaps,...) arranged on one side of the basin. The other sides can be simple walls, absorbing beaches or active absorbers.



Figure 1 ECN frontal wave tank

## 2.1.2 Corner

The Corner wave maker is composed of two front sides of wave maker elements. It allows to generate oblique waves of quality, exempting the experimental staff a rearrangement of the set-up (model orientation and/or moorings shifting) to test oblique wave excitation on the model. It can also generate more complex sea-states such as double peak spectra waves.

Shih and Chou (2009) ran numerical simulations of target oblique waves generated by two series of serpent-type wave generators set in L-shape (figure 2), also called dual-face snake-type wave maker (Park et al, 2001). This allows enlarging the effective testing area. Another type of generator, called the C-type multi-directional wave generator in accordance with its shape (figure 3), also enlarges the useful area (Ito et al., 1996) and has the following additional advantage: the wave makers can also absorb waves simultaneously, and therefore the basin can be used with different combinations of wavemaking and absorbing faces among the three sides.

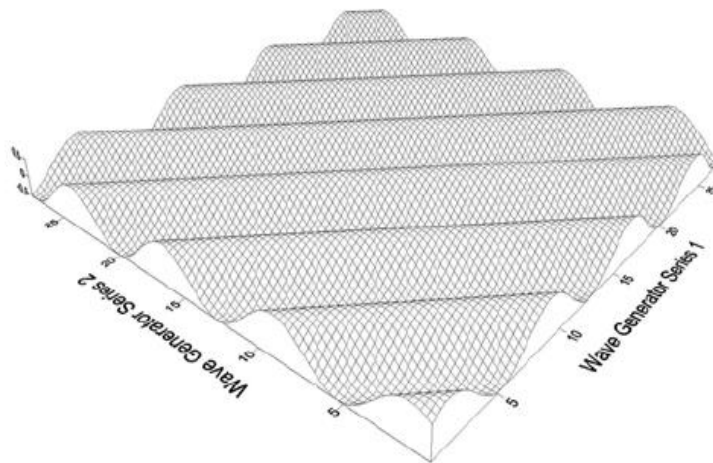
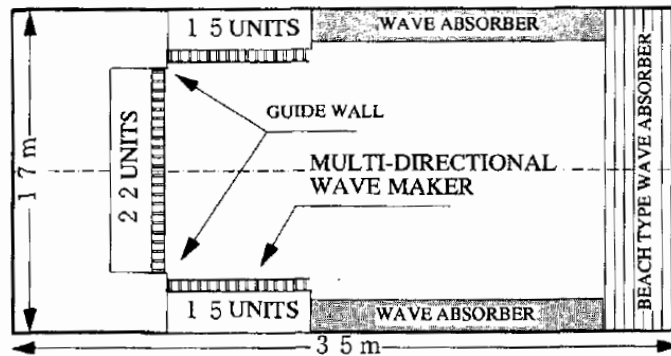
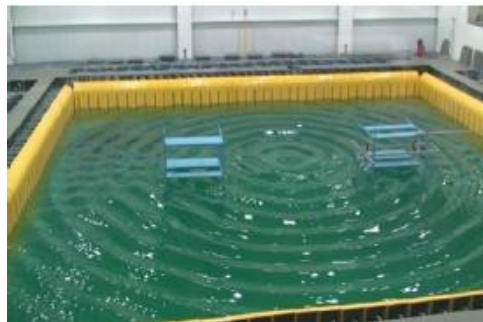


Figure 2 Spatial distributions of velocity in x-y planar for a regular wave when  $\theta = 45^\circ$  (Numerical solution) (Chih and Chou 2009).



**Figure 3 C-shape multi directional wave maker (Isobe 1996)**

The wave maker shown in figure 4 is the square tank of the University of São Paulo [3]. The 14m\*14m basin is equipped with 148 hinged-flaps.



**Figure 4 Picture of the square tank of the University of São Paulo**

Besides, real sea spectra often have two peaks of different directions of propagation. The two peak directions can be apart more than  $90^\circ$  each other, with a 'wind wave' component with relatively short periods and a 'swell' component with long periods. A Dual-mode snake type wave generator has been developed by Hiraishi and Hirayama (1998), which can generate directional waves with oblique principal direction and double-peak directional waves. However, Roux de Reilhac (2008) managed to generate double-peak spectra using a frontal wave maker. He used Molin methods, which are presented in section 4.

---

### 2.1.3 Curved / circular

Few facilities are equipped with a curved or a circular wave tank. The University of Edinburgh is equipped with both two types of tanks that will therefore be taken as an example of how work curved and circular tanks and what are their capacities in terms of device testing.

#### *Curved tank*

Firstly, the curved wave tank (figure 5) is a multi-directional wave facility, which is capable of producing digitally-controlled pseudo random waves with definable spectral and directional statistics. It is equipped with force feedback absorbing wave makers, which enhance the accuracy of marine environmental conditions through the minimisation of standing waves. The test facility is used to test systems in the range of scale 1:70 to 1:100 in a water depth of 1.2 m and the frequency range goes from 0.5 Hz to 2 Hz with a maximum trough to crest wave height of 0.22 m at 1Hz.

Directional waves by the curved wave tank are made possible through the principles of Huygens as illustrated in Figure 6. For the special geometry of the curved-tank, the motion of all wave makers with no phase delay generates a curved wave that propagates towards the centre of the wave makers arc. To produce a straight wave with a specified direction of propagation, each wave maker is addressed individually by the system controller, shifting its time response in the array by a certain delay ( $\gamma$ ) proportional to the sine of the angle ( $\alpha$ ) (Jorge Lucas PhD, 2011). More details are given in section 4.3.2.

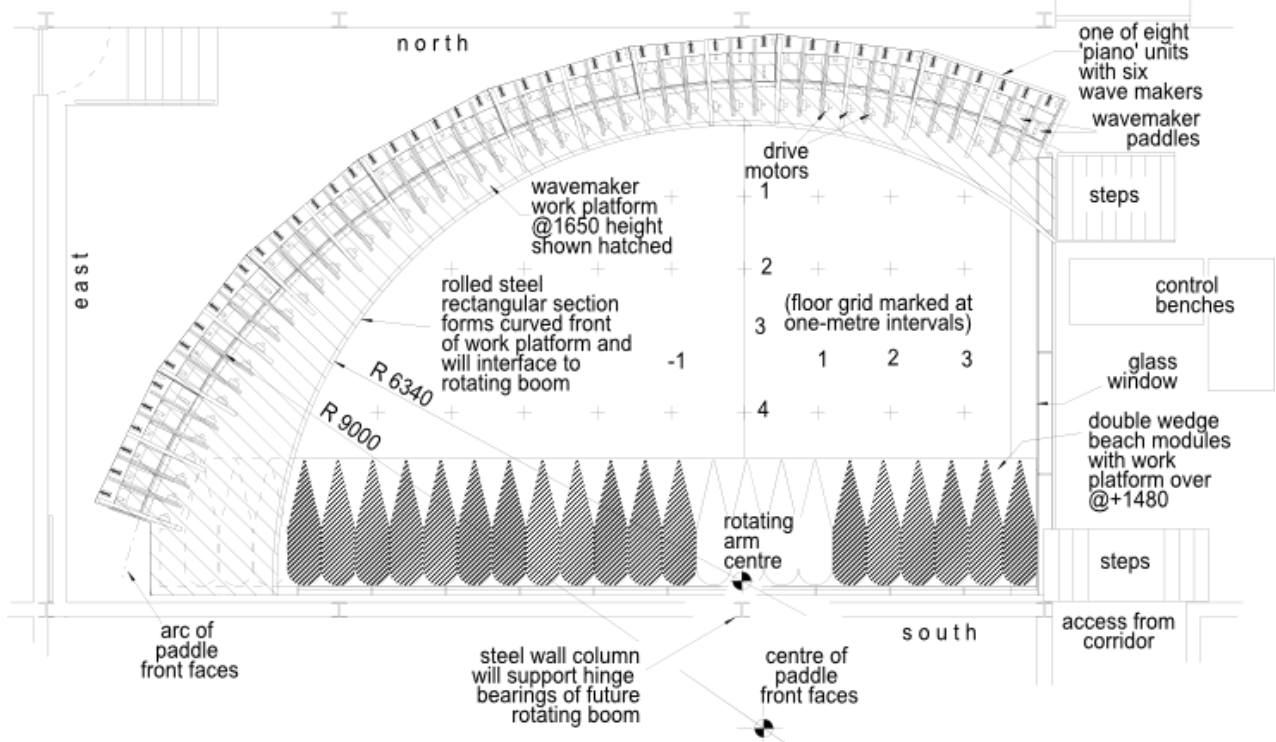


Figure 5 Plan view of the Curved Wave Tank (University of Edinburgh).

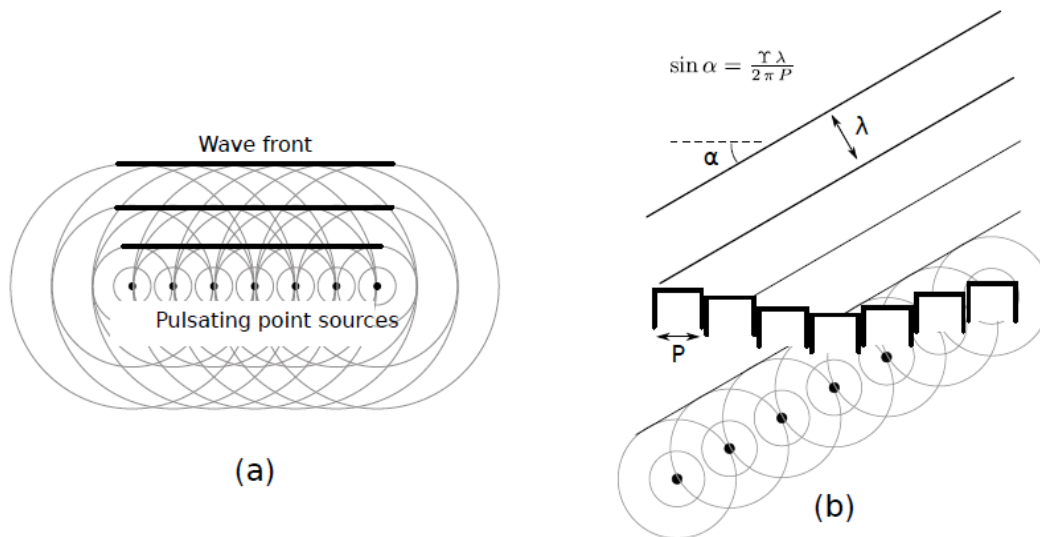


Figure 6 Illustration of the Huygens principle (University of Edinburgh).



---

Mixed seas in the curved-tank are generated by superimposing different ‘wave-fronts’. To produce a mixed sea in the curved tank, the random phase method is used. This method is deterministic and ensures that during different runs repeatable conditions occur. This is an important and desirable characteristic of wave generation for wave energy development.

### *Circular tank*

The All-Waters Combined Current and Wave Test Facility is a new basin which was constructed at the University of Edinburgh in 2013<sup>1</sup>. The tank has a diameter of 25m and a working depth of 2m (see figure 8 in section 3). The basin itself is approximately 5m deep with lower level containing the current generation hardware and plenum. It is designed to test models at a scale of approximately 1/20. 168 active absorbing paddle wave makers are located around the circumference of the tank. The wave makers absorb as well as generate waves and therefore the requirements for a conventional mesh/foam beach are greatly reduced. For regular unidirectional waves, it will be possible to reach heights of up to 0.7m at period of 1-2 seconds.

Besides, the installation of test models, whether moored or fixed, can be a time consuming and difficult process. In order to ease this operation and minimise downtime the central section of the tank floor (approximately corresponding the 15m diameter test area) can be raised out of the water to allow installation in dry conditions. A 5 tonnes overhead travelling crane allows models to be transported from the “quayside” onto the raised floor.

---

<sup>1</sup> The wavemaking and current generation infrastructure is supplied by Edinburgh Designs Ltd., a company that originated from University of Edinburgh.



The NMRI (National Maritime Research Institute) of Tokyo is equipped with a Deep Sea circular wave basin (figure 7) that generates current. The basin was constructed in 2002 because of the increasing demand for deep sea Oil & gas technology. More details are presented about this basin in section 3.1.

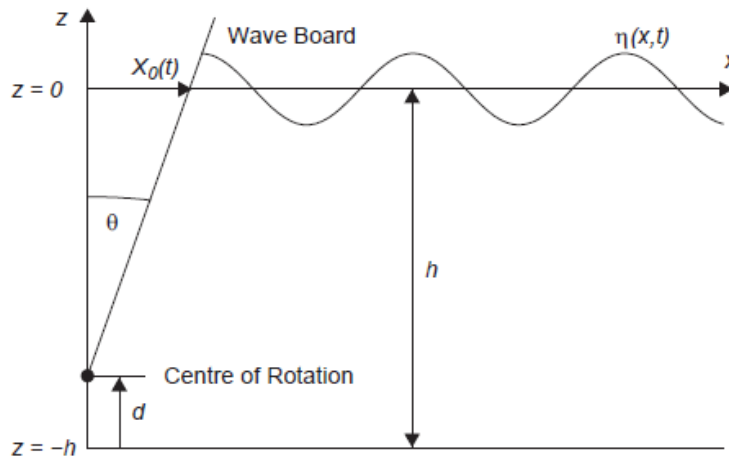


Figure 7 Deep-sea basin of NMRI Tokyo

## 2.2 DIFFERENT BY THEIR CONSTRUCTION

### 2.2.1 Hinged-flap type

Hinged-flap type wave makers are made with flat vertical plates hinged at the bottom and rotating around their axis so when driven with an oscillatory motion they partially rotate in a fore and aft arc. They are suited for physical modelling of deep water waves, where the water is barely perturbed at the lower depth of the tank. The pitching motion about the submerged hinge is regarded as more inductive to quickly produce the correct water particle orbital profiles which also exhibit the required exponential diameter decay with depth. If water depth changes are anticipated it can be possible to mount the flap generators on a movable frame that can be raised or lowered as required. Moreover, hinged-flap wave makers allow the installation of manifolds creating current flows. Hyun (1976) gave the first-order wave maker transfer function for the variable flap-type wave maker. More details can be found in S. A. Hughes's book (1993) [1]. Some facilities have flap paddles with an additional hinge at mid depth. Both sections can move independently such that almost pure sinusoidal water surface profiles can be produced.



**Figure 8 Wave maker geometry**

A wave maker is characterized by its transfer function  $TF(\omega)$ , which is defined as  $\mathbf{b} = TF(\omega) \mathbf{a}^2$  at the pulsation  $\omega$  and for a wave of direction  $0^\circ$ , with  $\mathbf{b}$  the wave maker amplitude and  $\mathbf{a}$  the wave amplitude.

The first-order transfer function for a paddle hinged (flap-type) at a distance  $d$  from the sea-bed is

$$TF_{2D} = -i \frac{k(h-d)}{4 \sinh(kh)} \frac{2kh + \sinh 2kh}{k(h-d) \sinh kh + \cosh kd - \cosh kh} \quad (2.1)$$

## 2.2.2 Piston-type

The piston-type wave maker is appropriate to generate shallow water waves. Indeed, as the wave board displacement is equal along the piston height, the water velocity is important even on the bottom of the basin, which is the particularity of shallow water dynamics. Moreover, piston-type wave makers accommodate water depth changes more easily than flap paddles. If there is water behind the wave maker in order to cancel hydrostatic forces, back waves are also generated behind the wave maker, which perturb the wave maker displacements. Edinburgh

<sup>2</sup>  $TF$  is defined herein as the opposite of the height-to-stroke ratio.

Designs Ltd. designed a piston wave maker that consists of two interconnected shapes that rotate relative to each other (figure 10). The rear surface of each of the components forms part of a cylinder centred on its axis of rotation, so no back wave is formed when the structure rotates. The largest force on the piston is the buoyancy followed by the wavemaking and the inertial forces due to acceleration. The structure should be light and corrosion resistant. The piston is designed for generation of shallow coastal waves of any type (from regular 2D -waves to short-crested<sup>3</sup> irregular waves) and can be used in tanks containing sediment as there are no seals, hinges or bearings in contact with the water. A great advantage is also that the wave maker can be easily moved anywhere in the basin.



Figure 9 'Classical' piston-type wave maker (Equimar)

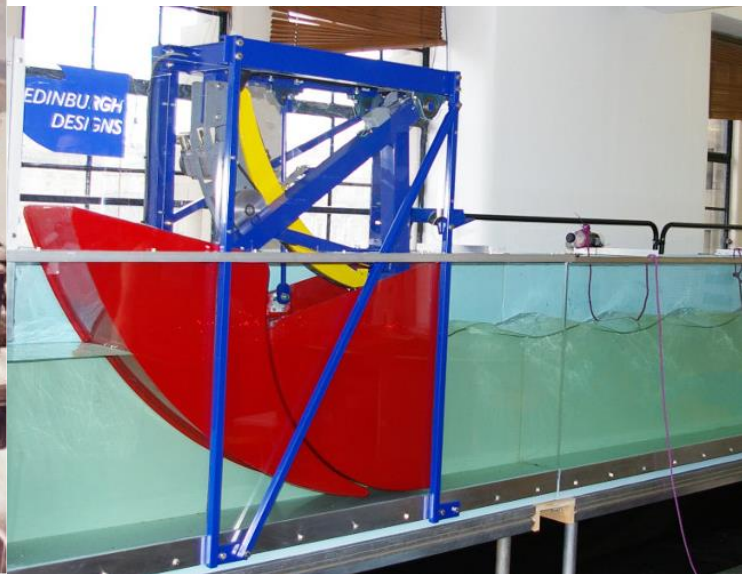


Figure 10 UCL piston - Images courtesy of EDL

The transfer function for a piston-type wave maker is obtained for  $d \rightarrow \infty$ , which transforms equation (2.1) into:

$$TF_{2D} = -i \frac{2kh + \sinh(2kh)}{4\sinh^2 kh} \quad (2.2)$$

<sup>3</sup> **Short-crested waves:** in the linear theory, short-crested wave fields are defined as a superposition of 2D progressive wave trains of equal wave lengths and frequency, propagating in two directions  $\theta_1$  and  $\theta_2$ .

### 2.2.3 Plunging-type

The plunger-type wave maker is a body free to oscillate vertically, such as illustrated in figure 11. This vertical motion displaces the fluid, creating the wave motion. The plunger can be of any shape but cylinders and triangular are most commonly used. According to Wang (1974), the wave height far from the plunger is not sensitive to its geometric details, apart from its width at  $z = 0$ , its draft in its neutral position and its cross-sectional area coefficient. An important factor for the wave generation is the water depth (parameter  $h$  in the wave maker transfer function), as for other generators.

This type of wave maker has several advantages, mostly practical and structural. Indeed, as its motion is purely vertical, the global machine is very compact. Moreover, as the shape is triangular, the basin can be designed to work with water behind the wave maker with almost no generation of back waves, which eliminate the usual problem of this configuration. An example of this type of basin is the Japanese wave tank AMOEBA (see section 4.3.).

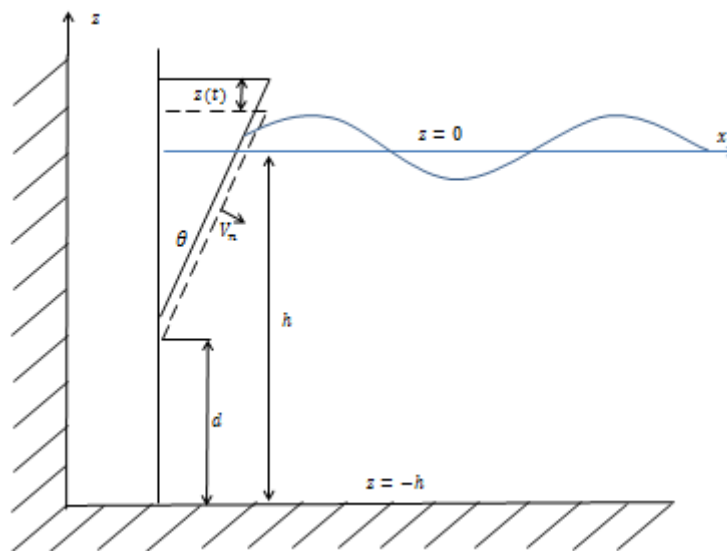


Figure 11 Plunger-type wave maker geometry

## 2.2.4 Duck-type

This type of wave maker is not as widely used as the others. It can be more efficient than other wave makers in theory but practically it is not the most convenient way of generating waves as it is potentially much more complicated to drive and the ratio of water displaced with respect to the dimensions are better for a piston-type than for a duck (figure 12).

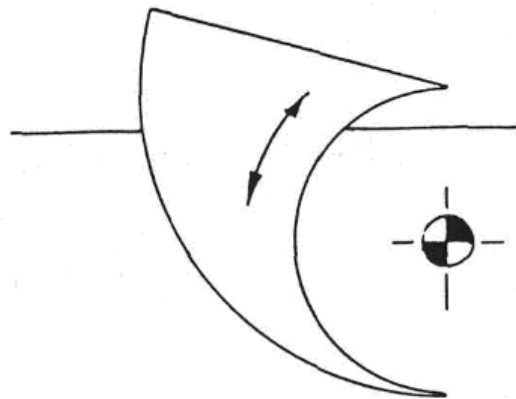


Figure 12 Duck-type (Salter 1981).

### 3 SIMULTANEOUS GENERATION OF WAVE AND CURRENT

This section describes the possibilities to generate simultaneously wave and current, through the presentation of three basins: the Deep sea basin of NMRI Tokyo, the All-waters combined current and wave test facility of the University of Edinburg (UEDIN) and the Ocean basin of the University of Plymouth (UoP).

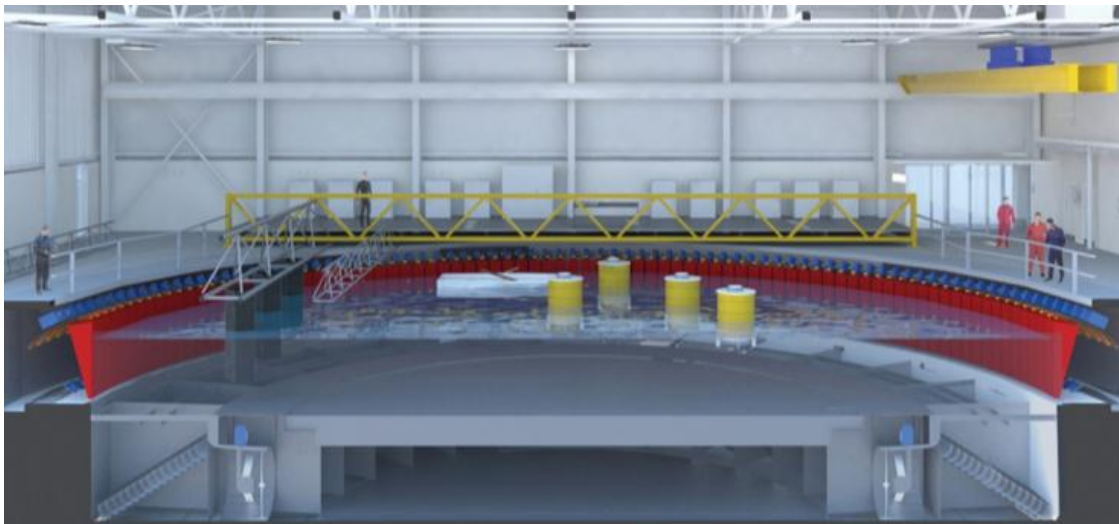


Figure 13 Architects' rendering illustrating major features of the All-Waters Combined Current and Wave Test Facility (image courtesy of Bennetts Associates Architects)



Figure 14 Picture of the Ocean basin in the University of Plymouth (UoP)

### 3.1 CURRENT GENERATION AND DIRECTIONALITY

The Deep sea wave basin of NMRI Tokyo (figure 15) is made of two parts: a circular basin with a 14m diameter and a deep pit of 30m depth, which makes this basin one of the deepest in the world. The tank is surrounded by 128 absorbing wave makers and current generators are installed both in the circular basin and in the deep pit.

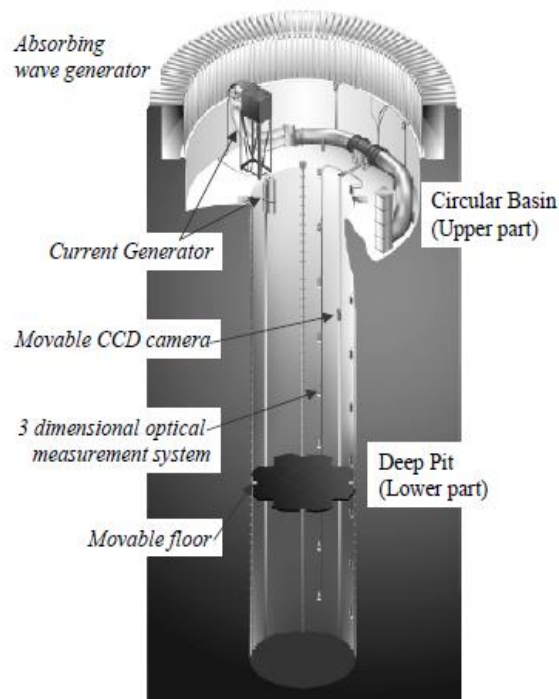


Figure 15 Deep sea basin at the NMRI Tokyo



The UEDIN circular basin is equipped with 28 impellor units located in a circular arrangement in the lower level of the tank basin. The maximum current velocity across the 15m diameter test section is 0.8 m/s. The flow is recirculated under the tank floor.

Concerning the UoP wave basin, it has a multi-pump recirculating hydraulic system that can generate longitudinal and transversal currents up to 0.3 m/s for a 2.0m water depth.

Tidal currents often do not exhibit a simple bidirectional flow. Devices will therefore not be subjected to tidal current along a single axis. In a test tank with a single direction (or axis) the test model must be repositioned and/or rotated to simulate the directional range of the tidal current. At best this is impractical, and in the case of a large array of devices it may be impossible. A preferable approach is to fix the position of the test models and vary the direction of the current. A circular tank provides the geometry to generate current in any direction in much the same way as it allows for the generation of complex multidirectional waves. The challenge is to develop a flow generation system that will provide a uniform velocity across the designated test area. This test area must also be suitably large to allow the installation of multiple models in order to allow the meaningful evaluation of device arrays. The test section proposed for the All-Waters facility (UEDIN) is a 60% of the overall diameter (15m out of 25 m). Combining the output from the impeller units (discrete) to form a uniform flow across the test section is a subject of on-going research involving small scale prototypes, CFD and control theory. The expected flow field is illustrated in Figures 16-17. Here a numerical model is used to predict how 28 individual centre pointing flow inlets can be controlled to produce a single one directional plan view flow in a round tank for array testing. (T. Davey et. al, 2012)

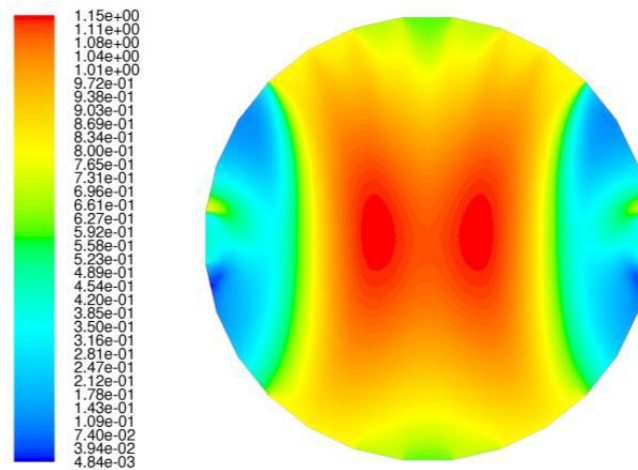


Figure 16 Contours of velocity magnitude across the tank (plan view), (University of Edinburgh).

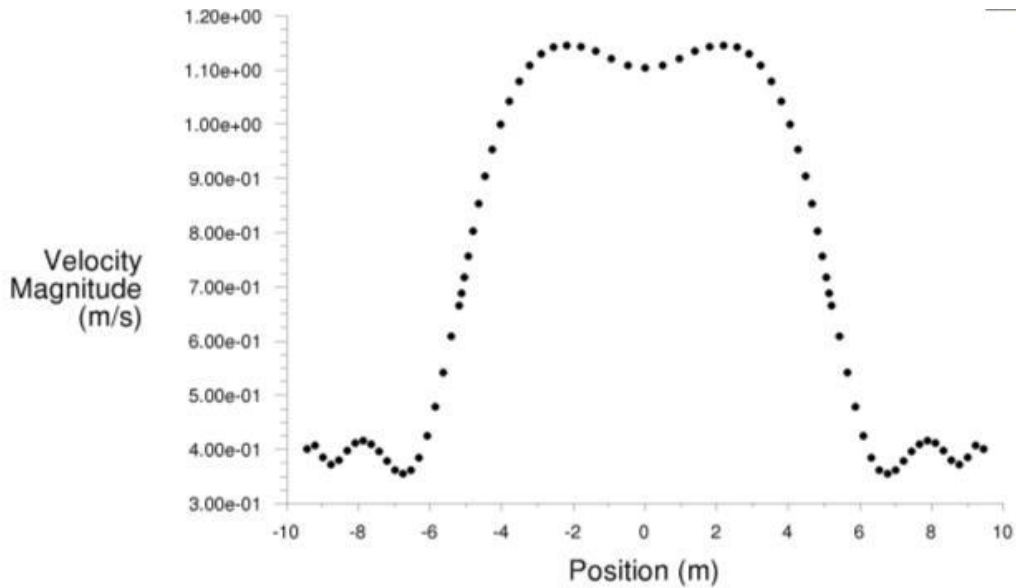


Figure 17 Velocity profile across the central section of the tank. (University of Edinburgh)

## 3.2 COMBINED WAVE AND CURRENT

The circular design of UEDIN's basin with 360° symmetry allows the waves and current to be generated in any relative direction. The flow conditioning system (for the current) is being developed to minimise the velocities immediately in front of the wave makers, thus allowing the active absorption systems to operate correctly in a combined wave and current sea.

Besides, the University of Plymouth's wave flume can generate simultaneously a reversible flow recirculation of 0.5 m/s along the flume and waves up to 0.35m height. In addition to this, sediments can be introduced for special tests.

The effect of marine current on WECs (wave energy converters) is not well documented yet, as only few facilities offer the possibility to test waves and current of these magnitudes simultaneously.

An investigation was carried by Hiraishi (2002) to assess the influence of current action on the directional spectrum variation. The investigation has its importance since the current magnitude in shallow water areas can become significant, leading to wave directionality modifications. Such influences affect the wave loads applied to a structure as the external wave forces depend on directionality (Hiraishi 2001).

The directional spectrum in the case of opposed current action shows higher peak than without current. The peak angle is almost same to the target wave direction ( $-15^\circ$ ). Meanwhile the directional wave spectrum in the following current gives lower peak than without current. The observed differences demonstrate that the wave energy concentration is raised in the opposing currents and is decreased in the following flows. The wave energy is concentrated in the principal direction of propagation when waves progress against the current. This is caused by the refraction of wave components that proceed in oblique directions. Along those lines, the oblique components may be shifted near the parallel direction to the current in case of the following current.

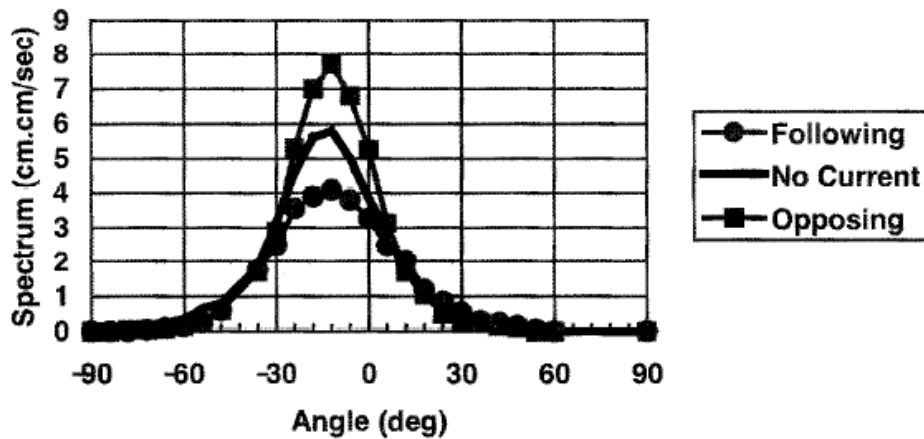


Figure 18 Variation of directional spectrum under current action (Hiraishi 2002)

## 4 RANDOM WAVE SIMULATION

### 4.1 FREQUENCY SPECTRUM

To generate irregular waves in a wave tank, a command signal has to be sent to the wave maker control system. But previously to that, the wave elevation time series corresponding to the desired sea-state must be computed. This section focuses on the different techniques available to compute these time series.

The different techniques can be classified into two methods: ‘deterministic’ and ‘non-deterministic’ (or ‘probabilistic’).

#### 4.1.1 Deterministic techniques.

Deterministic wave generation techniques create wave trains of finite duration (periodic) which match the target energy spectrum on a period of repetition.

##### 4.1.1.1 Random Phase Method.

The Random Phase Method was developed by Rice in 1944.

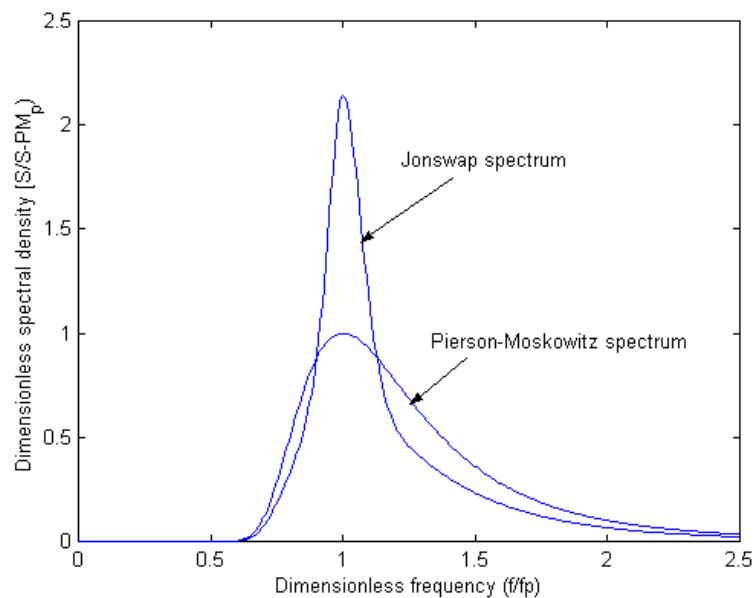


Figure 99 Wave spectra examples

When dealing with irregular waves, the waves can be described by a power spectral density  $S(f)$ . A representation of two particular wave spectra is given in figure 19. If the wave steepness is sufficiently small, the assumption of linear irregular waves can be done. Therefore, the surface elevation can be described as a superposition of wave components of different frequencies:

$$\eta(t_j) = \sum_{i=1}^N \eta_i(t_j) = \sum_{i=1}^N a_i \cos(\omega_i t_j + \varphi_i) \quad (4.1)$$

where  $\omega_i = 2\pi f_i$

$a_i$ : Fourier amplitude spectrum coefficient (amplitude of the wave component of frequency  $f_i$ ).

$\varphi_i$ : random phase.

$t_j$ :  $j^{th}$  component of the time vector.

The smooth spectrum is subdivided in equal frequency increments of width  $\Delta f$  over the range of frequency  $[0, f_{max}]$ . The maximum frequency  $f_{max}$  will control the time step width through  $\Delta t = \frac{1}{2f_{max}}$ .  $f_{max} = f_N$  is chosen to get a number of samples  $N$  that is a power of 2 in the FFT. Moreover,  $\Delta f$  is chosen such that  $\Delta f = \frac{1}{T_R}$ , where  $T_R$  is the length of the time series to be produced.  $T_R$  also corresponds to the repetition period of the time series.

The relation between the spectrum energy and the linear approximation variance is given by:

$$\int_0^{\infty} S(f) df \cong \sum_i S(f_i) \cdot \Delta f = \sum_i \frac{1}{2} a_i^2 \quad (4.2)$$

Hence

$$a_i = \sqrt{2S(f_i) \cdot \Delta f} \quad (4.3)$$

The phase  $\varphi(f_i)$  is chosen randomly at each frequency  $f_i$  with a uniform probability distribution between 0 and  $2\pi$ . However, the phase generation is controlled by a 'seed' so that the same series of phase values are created when the seed is kept constant.

The target time series is obtained by an Inverse Discrete Fourier Transform (IDFT)

$$\eta_j = \sum_i a_i \cos(\omega_i t_j + \varphi_i) \quad (4.4)$$

The Random Phase Method is considered 'deterministic' because the time series output are completely defined by the specified target spectrum and the seed parameter.

#### 4.1.1.2 Pros and cons of this deterministic method.

The discretized spectrum of the generated wave train is equal (neglecting the non-linear effects) to the target energy spectrum during a repetition period  $T_R$ . This means that two different realizations with different properties can be directly compared and two different devices can be compared under the same sea-state (repeatability).

However, the wave trains generated do not reproduce the true random behavior of the ocean waves. Indeed, extreme events of low probability that might happen in the real world can be missing. What is done in most facilities using this method is that extreme events are generated separately in a deterministic manner. Therefore, the only limit of proceeding that way is that more complex extreme events than large amplitude waves can occur, and these events might be difficult to predict.

### 4.1.2 Non-deterministic techniques

#### 4.1.2.1 Random Complex Phase Method.

In the so-called method developed by Borgman (1969, 1979) and described later by Tuah and Hudspeth (1982), the Fourier coefficients  $a_i$  are statistically independent. They are obtained by multiplying the square root of the spectral density values  $S(f_i)$  by a random variable  $G$  having a Gaussian distribution with zero mean and standard deviation of 1:

$$a_i = G_j \cdot \sqrt{\frac{S(f_i)\Delta f}{2}} \quad (4.5)$$

Then, the target time series is obtained by an Inverse Discrete Fourier Transform (IDFT) as in 4.1.1.1.

This 'filtering' operation conserves the energy spectrum in terms of probability only, and for very long periods of time (theoretically infinite).

#### 4.1.2.2 White Noise Filtering Method.

With this method [Nunes (1981)], the time series is obtained by generating a white noise signal<sup>(1)</sup>  $W(t)$  which is convolved with the discrete target wave spectrum  $S(f_i)$ :

$$\eta_j = \sum_{i=1}^N W_{j-i} \cdot \sqrt{\frac{S(f_i)\Delta f}{2}} \quad (4.6)$$

where  $N$  denotes the number of Fourier coefficients.

### 4.1.2.3 Pros and cons of the non-deterministic methods

Non-deterministic techniques produce wave trains which only match the spectrum in terms of probability for runs of infinite durations. Practically, this means that experimental runs have to be sufficiently long to properly represent the target spectrum. Miles & Funke (1989) have shown that even 20 minutes realizations can deviate very significantly from the target spectrum when using non-deterministic methods.

## 4.2 DIRECTIONAL SPECTRUM

Oblique or three-dimensional waves are two different appellations which designate waves having a direction of propagation different from the longitudinal axis of the basin. Their generation is achieved using a segmented wave maker and the direction of propagation of the oblique waves depends on the wave maker's paddles motion.

A directional sea-state is described mathematically by a superposition at the considered location in the basin of incident wave components of different frequencies and directions. Thus, an irregular short-crested wave train is a superposition of long-crested waves of different directions. The frequency and direction contributions of the energy spectrum  $S(\omega, \theta)$  are usually considered as mutually independent and expressed as follows:

$$S(\omega, \theta) = S(\omega)D(\omega, \theta) \quad (4.7)$$

where  $D(\omega, \theta)$  is the directional spreading function which verifies  $\int_{-\pi}^{\pi} D(\omega, \theta) d\theta = 1$  (4.8)

Two methods are available in order to compute the directional sea-spectrum: the single and the double summation methods.

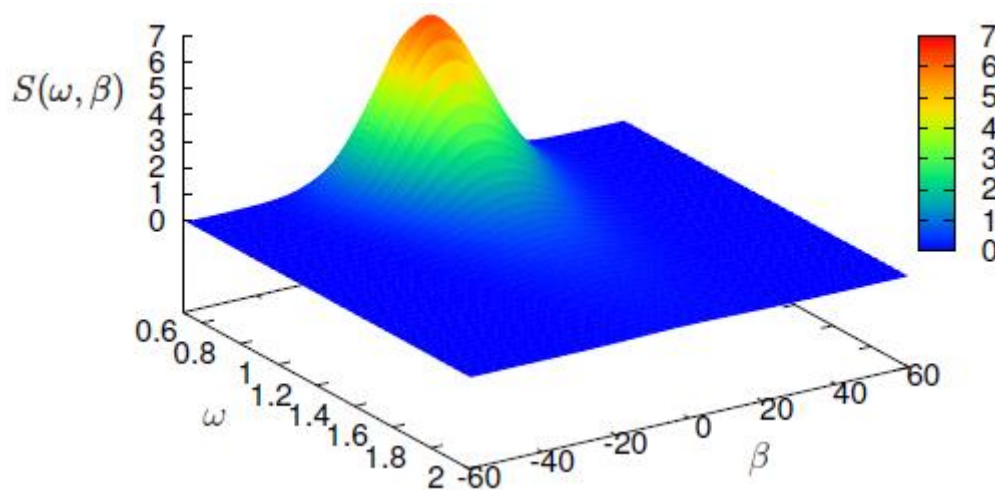


Figure 20 Directional spectrum. (M. Philippe 2012)

### 4.2.1 Double summation method

This method [Forristall (1981), Pinkster (1984)] was originally the most commonly used for generating multi-directional waves in tanks. The water surface elevation is defined by the following formula:

$$\eta(x, y, t) = \sum_{i=1}^N \sum_{j=1}^M a_{ij} \cos(k_i(x \cos \theta_j + y \sin \theta_j) - \omega_i t + \varphi_{ij}) \quad (4.9)$$

where  $(a_{ij}, \varphi_{ij})$  are the couples of amplitude-phase of wave components having frequencies  $\omega_i$  and directions  $\theta_j$ , and  $(x, y)$  are horizontal spatial coordinates.

Equation (4.9) means that the irregular short-crested wave field is built by  $N \cdot M$  wave fronts. The main issue encountered with this method is that for each of the  $N$  frequencies  $\omega_i$ ,  $M$  wave fronts are generated, of different directions  $\theta_j$  but having exactly the same frequency, leading to 'phase locking'.

### 4.2.2 Phase locking phenomenon

Two waves (at least) are phase-locked when they have the same frequency  $\omega_i$  but a different phase  $\varphi_{ij}$ . However, they can have different directions of propagation  $\theta_j$ . The resulting wave field has nodes and antinodes and is therefore spatially inhomogeneous and non-ergodic [Jeffreys (1987)]. This means that the wave field will have different statistical properties from one point of the basin to another. The practical consequences of a non-homogeneous wave field can be observed when drift force and low frequency mooring oscillations move the device away from its original location, where the wave behavior may be different: the device response is different from expected. More information on the impact of non-ergodicity and inhomogeneity can be found in Jeffreys (1987).

### 4.2.3 Single summation method

The alternate method [Miles & Funke (1989)] generates a single wave component for each frequency, which leads to a spatially homogeneous and ergodic wave field and avoids phase-locking. The surface elevation is defined by:

$$\eta(x, y, t) = \sum_{i=1}^N a_i \cos(k_i(x \cos \theta_i + y \sin \theta_i) - \omega_i t + \varphi_i) \quad (4.10)$$

where 
$$\omega_i = i \frac{\Delta\omega}{M} \quad (4.11)$$

and with  $M$  the number of directions of propagation. Therefore, each component has a different frequency and all the directions  $M$  are included in each frequency bandwidth  $\Delta\omega$ .

Obviously, the more  $M$  is increased or  $\Delta\omega$  is reduced, the more the waves computed with this method are consistent with the continuous target wave spectrum. However, these parameters value are limited by the angular and the frequency resolutions of the wave making system.



### 4.3 NON-LINEAR EFFECTS

The deterministic and non-deterministic methods described above rely on the assumption of linear waves. This assumption is valid if the wave steepness is small enough. Steepness is defined respectively for regular and irregular waves as follows:

$$ka \quad \text{and} \quad \frac{K_p H_s}{2\sqrt{2}}$$

If the steepness is too important, non-linear phenomena might appear. For instance, some contribution of the spectrum can be shifted towards the high frequencies.

However practically, these issues can be fixed by recalibrating the wave maker. Indeed, the measured and target directional spectra are compared, and the difference between them is reduced using an iterative process.

---

## 5 ON THE ACCURATE GENERATION OF A SEA-STATE ON A GIVEN AREA OF THE TANK.

Different methods to compute the wave spectrum have been described in the last section. It has been seen that in the case of a directional irregular wave field, the surface elevation of the target wave (the wave to be generated) in any location of the basin is described as a sum (simple or double) of wave components of different frequencies and directions. Now, the wave maker's command needs to be computed and this may be achieved through several methods. This section aims to present famous and simple methods as well as more innovative and elaborated ones.

### 5.1 THE SNAKE'S PRINCIPLE

#### 5.1.1 Basic snake's principle

The Snake's principle is the simplest method to generate oblique waves, and it was proposed by Biésel in 1954. The method takes its name from the fact that the paddles' motion has a sinusoidal shape in the  $y$  direction (figure 22).

First of all, the parameters of the oblique wave must be introduced. The formula below gives the relation between the direction of propagation  $\theta$ , the wave number  $k$  and  $k'$ , and the corresponding wave lengths  $L$  and  $L'$  and figure 21 provides a geometrical representation of oblique waves generated by a segmented wave maker.

$$\sin \theta = \frac{k'}{k} = \frac{L}{L'} \quad (5.1)$$

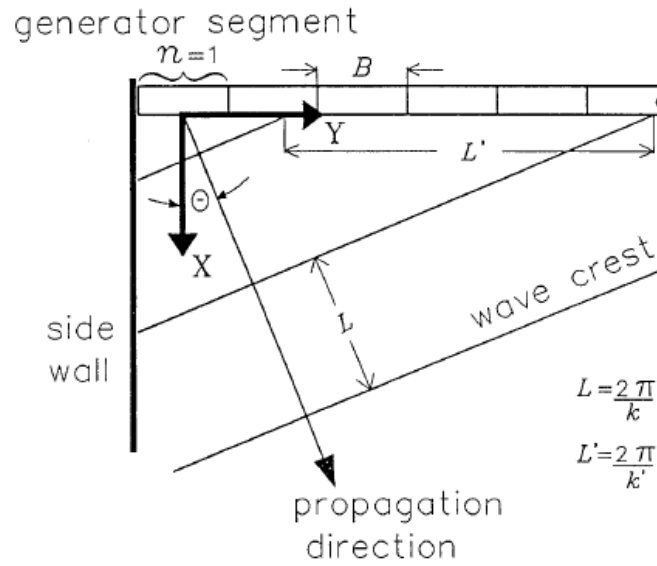


**Figure 21** Definition of coordinate system, plan view. (D. Shaver, M., 1989)

In the case of a wave maker infinite in the  $y$  direction, the expression of the continuous wave maker's displacement required to generate an oblique wave of direction  $\theta$  is given by

$$X(y, z) = \mathbf{b}g_v(z)e^{-ikysin\theta} \quad (5.2)$$

where  $g_v(z)$  is the vertical shape of the wave maker and  $\mathbf{b}$  is the amplitude of the wave maker's motion.

For a segmented wave maker (real wave maker) composed of several paddles, the expression of the wave maker's displacement becomes:

$$X_s(y, z) = \sum_{n \in \mathbb{Z}} \frac{\sin \tau}{\tau - n\pi} e^{-i(k \sin \theta - \frac{2\pi n}{B})y} \quad (5.3)$$

with  $\tau = \frac{1}{2}kBs \sin \theta = \frac{1}{2}k'B.$  (5.4)

The expression (5.3) is found doing a decomposition of an exponential function into a Fourier series. More details can be found in F. Bonnefoy's thesis (2005).

The segment width to wavelength ratio  $\frac{B}{L}$  must be sufficiently small, to avoid the generation of secondary propagating wave components. According to Biésel, the condition to achieve this is to have

$$\frac{B}{L} \leq \frac{1}{\sqrt{2+|\sin \theta|}} \quad (5.5)$$

This condition to avoid a spurious mode due to the segmentation concerns the short wave numbers and depends on the direction of propagation. For the  $0^\circ$  angle waves, the paddle width has no influence, as expected.

Then to relate the surface elevation for oblique waves to the wave maker's displacement, the three-dimensional transfer function must be defined. The relation between the 2D and the 3D transfer function is expressed as follows:

$$TF_{3D} = \cos \theta TF_{2D} \quad (5.6)$$

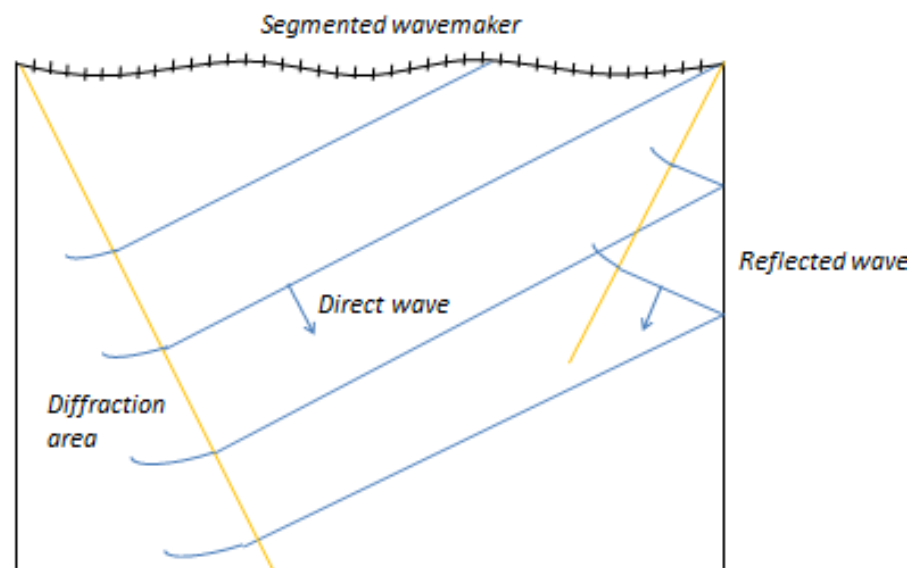


Figure 22 Illustration of the Snake's principle

Then, superposing several regular oblique waves of different frequencies, one can generate target regular or irregular multi-directional wave fields, as described in section 4. In this case, each wave component of the sums (4.9) or (4.10) must be multiplied by the transfer function  $TF_{3D}^f$ . However, a limitation to the generation of multi-directional sea states in a finite basin is the small size of the useful area over which we effectively observe the target wave field. Indeed, using the simple snake method, the target wave field is applied on the wave maker (at  $x = 0$ ), and the waves are reflected on the side walls what perturb the wave field in the testing area (useful area). This aspect has been considered by Sand and Mynett (1987) and subsequently by Funke and Miles (1987) who built methods taking into account these reflections on the side walls in order to get both a better quality of wave and a larger testing area.

### 5.1.2 Corner method Funke & miles (without diffraction)

The first method developed taking into account the reflections on the side walls to generate oblique waves is the corner method (Funke & Miles 1987). This straightforward method consists in determining three parts along the wave maker's width: a group of wave maker elements that do not move (3 in figure 23), another that generates waves of direction  $\theta^\circ$  (2), and a third that generates both waves of direction  $-\theta^\circ$  and  $\theta^\circ$  (1) in order to get only waves of direction  $\theta^\circ$  in a desired area of the basin. Figure 23 illustrates the direction of the waves in each part of the basin and figure 24 represents the wave maker displacement along the transversal direction  $y$ .

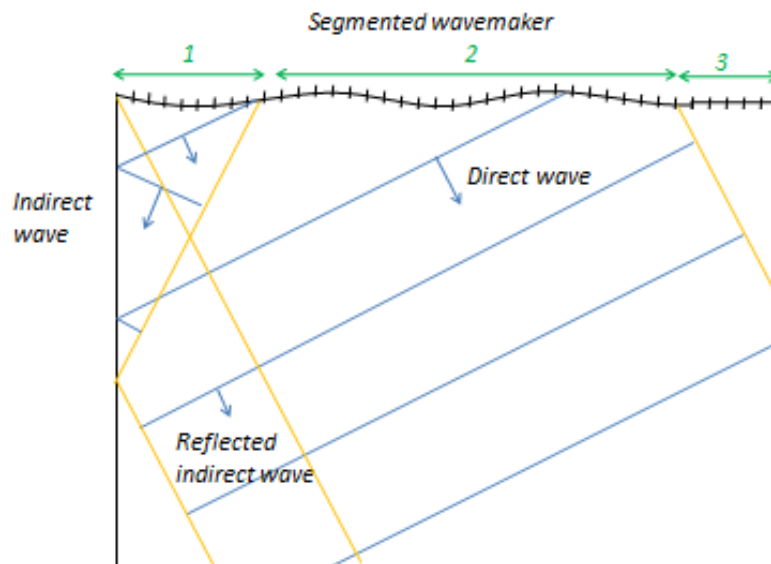


Figure 23 Illustration of the corner method

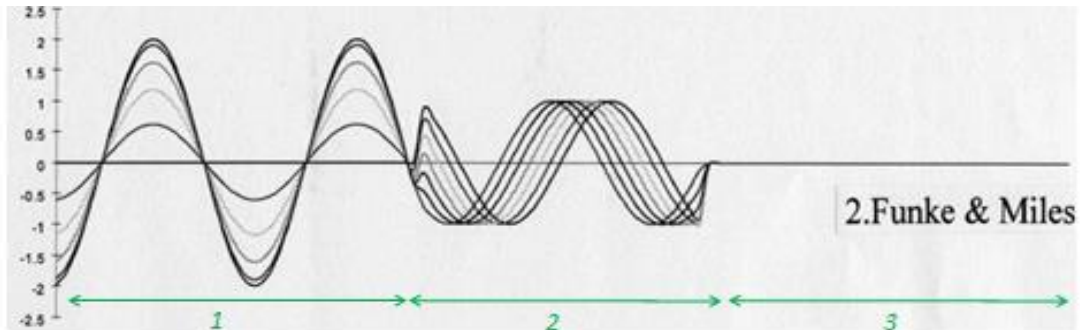


Figure 24 Wave maker's position along the transverse direction at different times (Boudet and Perois 2001)

Figure 25 shows the surface of the useful area for the Snake (left) and the Corner method (right). It appears clearly that the Corner method enables an enlargement of the useful area.

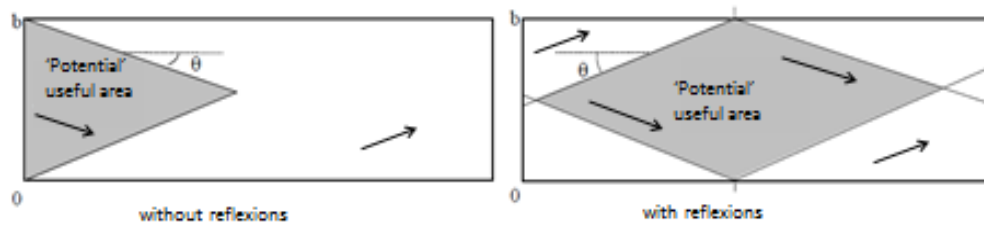


Figure 25 Useful area geometry for a wave of direction  $\theta$  (the arrows represent the wave direction (Boudet and Perois 2001).

## 5.2 ELABORATED METHODS

### 5.2.1 Principle

The generation of oblique elementary waves using linearized potential theory at the first order consists in reproducing a target wave field. Surface elevation (5.7) and potential (5.8) are expressed in a tank of infinite spatial dimensions:

$$\boldsymbol{\eta}_1 = \mathbf{a} e^{-ik(x\cos\theta + y\sin\theta)} \quad (5.7)$$

$$\phi_1 = \frac{i\mathbf{a}}{\omega} F^+(\alpha_0, z) e^{-ik(x\cos\theta + y\sin\theta)} \quad (5.8)$$

where  $\mathbf{a} = \mathbf{a} e^{i(\omega t + \varphi)}$  is the time-dependent amplitude vector.

Obviously,  $\boldsymbol{\eta}_1$  in (5.7) is the surface-elevation for one regular oblique wave. However, for a short-crested target wave field, (5.7) becomes the sum of wave components described in section 4:  $\boldsymbol{\eta} = \sum_{i=1}^N \mathbf{a}_i e^{-i(k_i(x\cos\theta_i + y\sin\theta_i) - \omega_i t - \varphi_i)}$ . The decomposition described below must be applied for each wave component  $\mathbf{a}_i e^{-i(k_i(x\cos\theta_i + y\sin\theta_i) - \omega_i t - \varphi_i)}$  of the sum.

The solution in a finite tank of width  $L_y$  in steady state is a superposition of the elementary spatial modes of the tank in order to approximate the infinite one.

$$\boldsymbol{\eta}_{finite} = \sum_{m=0}^{+\infty} \sum_{n=0}^{+\infty} \mathbf{a}_{mn} e^{-k_{mn}x} \cos(\mu_n y) \quad , \quad \text{with } \mu_n = \frac{n\pi}{L_y}, \quad n \in \mathbb{N}, \quad (5.9)$$

$$\phi_{finite} = \sum_{m=0}^{+\infty} \sum_{n=0}^{+\infty} \frac{i\mathbf{a}_{mn}}{\omega} e^{-k_{mn}x} \cos \mu_n y F^+(\alpha_m, z) \quad (5.10)$$

with  $F^\pm(\alpha_m, z) = \frac{e^{i\alpha_m(z+1)} \pm e^{-i\alpha_m(z+1)}}{e^{i\alpha_m} + e^{-i\alpha_m}}$ , where the wave numbers are defined by  $k_{mn}^2 = \alpha_m^2 + \mu_n^2$ , where the vertical wave numbers  $\{\alpha_0 = ik, \alpha_m \in \mathbb{R}\}$  are the roots of the dispersion relation  $\omega^2 = i\alpha_m F^-(\alpha_m, 0)$ .

The vertical geometry  $g_v(z)$  of the wave maker is different from the velocity profile of the generated wave (figure 26). As a result, evanescent waves are generated close to the wave maker but their contribution decays quickly (in  $\exp(-kx)$ ) and has an influence until more or less twice the depth. Therefore, their contribution can be neglected in the testing area (see [11] for further details).

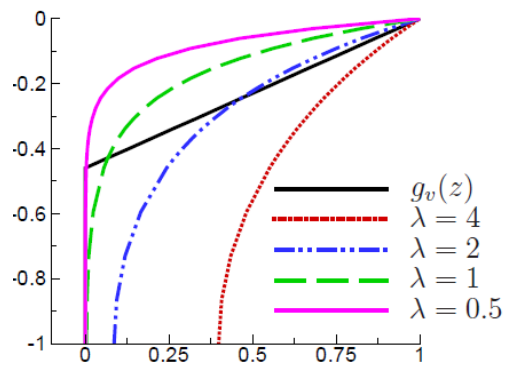


Figure 26 Vertical profile;  $\lambda$ : wavelength (m). (Bonney 2005)



Both progressive waves and evanescent modes appear in the potential expression (5.10). The vertical wave numbers  $\alpha_{mn}$  are purely imaginary or real positive respectively for progressive waves and evanescent modes. Progressive waves correspond to the restricted domain  $m = 0$  and  $n \leq E \left[ \frac{kb}{\pi} \right] = N_1$  (where  $E \cdot$  is the integer value) and evanescent waves to all other couples of  $(m, n)$  subscripts.

**Table 1**

$m = 0$		$m \geq 1$	
$n \leq N_1$	<i>progressive</i>	$n \in \mathbb{N}$	<i>evanescent</i>
$n > N_1$	<i>evanescent</i>		

Practically, the wave maker motion is calculated using a set of complex amplitudes  $\underline{a_{0n}}$ , which are the only unknowns of the problem:

$$\mathbf{X}_1(y, z) = g_v(z) \mathbf{TF} \sum_{n=0}^{N_1} \mathbf{a}_{0n} \cos \theta_n e^{-iky \sin \theta_n} \quad (5.11)$$

Where the  $\theta_n$  represent the natural modes directions given by  $\theta_n = \arcsin \frac{\mu_n}{k}$ .

Expression (5.11) means that the wave maker motion  $\mathbf{X}_1$  can be represented by the spatial modes.

The unknowns  $\mathbf{a}_{0n}$  are determined using the four elaborated methods that are presented hereafter.

**NB:** Equations (5.9) & (5.10) describe respectively the surface elevation and the wave potential effectively generated by the wave maker (including evanescent waves), whereas (5.11) expresses the required wave maker displacement (only progressive terms) that gives this wave field. Indeed, the evanescent waves are a consequence of the wave maker non perfect shape and are not taken into account in the wave maker command.

## 5.2.2 Presentation of four elaborated methods

### 5.2.2.1 Dalrymple's method (1989)

Dalrymple proposed an expression that uses voluntary reflections on the side walls with the same motivation as Funke & Miles: to extend the area of the useful zone. The idea is to impose the target field on a line parallel to the wave maker and located at a distance  $X_d$  from it. The method gives the amplitudes of the  $\mathbf{a}_{0n}$  coefficients:

$$\mathbf{a}_{0n} = \mathbf{a} I_n e^{i(k_{0n} - \alpha_0 \cos \theta) X_d} \quad (5.12)$$

where

$$I_n = \frac{\int_0^{L_y} e^{-ik \sin \theta y} \cos(\mu_n y) dy}{\int_0^{L_y} \cos^2(\mu_n y) dy} \quad (5.13)$$

Once these coefficients are calculated, equation (5.11) gives the wave maker motion.

### 5.2.2.2 Method of the disk-shaped area

Developed by Molin (1991), this technique also uses voluntary reflections on the side walls of the wave tank. The target amplitude is generated on a disk-shaped area instead of on a line. One of the advantages of this method is that it doesn't try to get the right target close to the walls (that has no practical use) but prefer to improve the quality in the middle of the tank where the models are tested.

Keeping only the progressive part (as in expression (5.11)) a potential as close as possible from a regular wave of direction  $\theta$  must be sought. Thereby, one can define the quantity  $A(r, \beta)$  that represents the difference between the generated wave field and the target.

$$\mathbf{A}(r, \beta) = \sum_{n=0}^{N_1} \mathbf{a}_{0n} e^{-k_{0n}(x_0 + r \cos \beta)} \cos(\mu_n(y_0 + r \sin \beta)) - \mathbf{a} e^{-ik((x_0 + r \cos \beta) \cos \theta + (y_0 + r \sin \beta) \sin \theta)} \quad (5.14)$$

Afterwards, Molin [20], [21] seeks a solution  $\mathbf{a}_{0n}$  that minimizes the difference  $\mathbf{A}$  on the disk using a least-square method. So practically, he minimizes  $I_1$ . After he remarked several times the apparition of unrealistic amplitudes, Molin added a second quantity  $I_2$  that limits the wave maker power. Therefore, the relevant quantity to minimize became  $I = I_1 + I_2$ .

$$I_1 = \int_0^{2\pi} \int_0^R \mathbf{A}(r, \beta) \mathbf{A}^*(r, \beta) r dr d\beta \quad (5.15)$$

$$I_2 = C \int_0^{L_y} \int_{-h}^0 \phi_x \phi_x^* dy dz \quad (5.16)$$

### 5.2.2.3 Method of the rectangular area

Also developed by Molin, this method allows to generate a useful area that has a rectangular shape. *A priori*, both Dalrymple and disk generating methods seem appropriate to test moored models whereas the method of the rectangular area seems more relevant for models with an advance speed.

The approach is similar to the method of the disk-shaped area. Indeed, it minimizes the difference  $F(x, y)$  between the generated wave field and the target in the target area.

$$\mathbf{F}(x, y) = \sum_{n=0}^{N_1} \mathbf{a}_{0n} e^{-k_{0n}x} \cos(\mu_n y) - e^{-ik(x\cos\theta + y\sin\theta)} \quad (5.17)$$

The coefficients  $\mathbf{a}_{0n}$  are obtained minimizing the function  $I$ .

$$I = \int_{x_1}^{x_2} \int_{y_1}^{y_2} \mathbf{F}(x, y) \mathbf{F}^*(x, y) dx dy \quad (5.18)$$

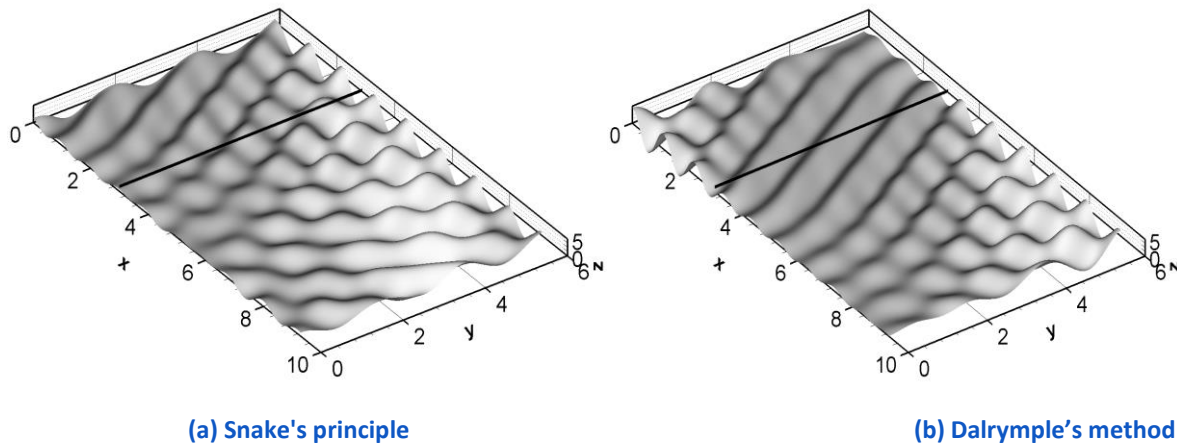
### 5.2.2.4 Method Segment by Segment

This method requires first to calculate the wave field induced by the unitary displacement of each wave maker element taken separately. Then, the method minimizes the difference between the generated wave field and the target using a least-square method as for the disk and rectangular methods. That gives the correct amplitude and phase of each wave maker segment. This optimization is made on some points of the free surface that belong to a control surface with an *a priori* arbitrarily geometry.

### 5.2.2.5 Pros and cons of the different methods

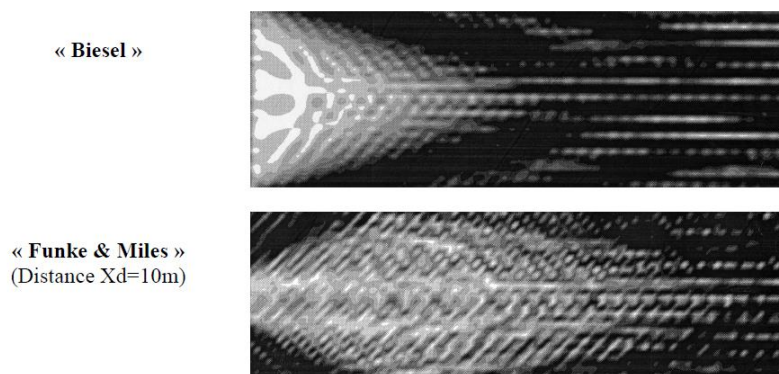
#### *Regular waves*

Figure 27 shows that the direction of propagation of the waves is not well reproduced by the Snake's principle due to the reflexions on the side wall ( $y=6$ ). The useful area is very limited in front of the wave maker and it is perturbed by the evanescent modes. In contrast, Dalrymple method with a target distance of  $X = 3$  provides a wave field which is clearly better reproduced.



**Figure 27** First order wave field with  $f=0.4\text{Hz}$  and  $\theta=30^\circ$ . (Bonnetoy 2005)

The white areas on figure 28 correspond to an error on the wave amplitude lower than 5%. The wave maker is located on the left side. In both cases, the useful area has the expected shape but the generated wave field is not really homogeneous because of the diffraction phenomenon.



**Figure 28** Error between generated wave fields and targets (Boudet and Perois 2001)

Figure 29 illustrates the displacements of the wave maker elements, for three different methods of command, at different moments and for the same target wave field.

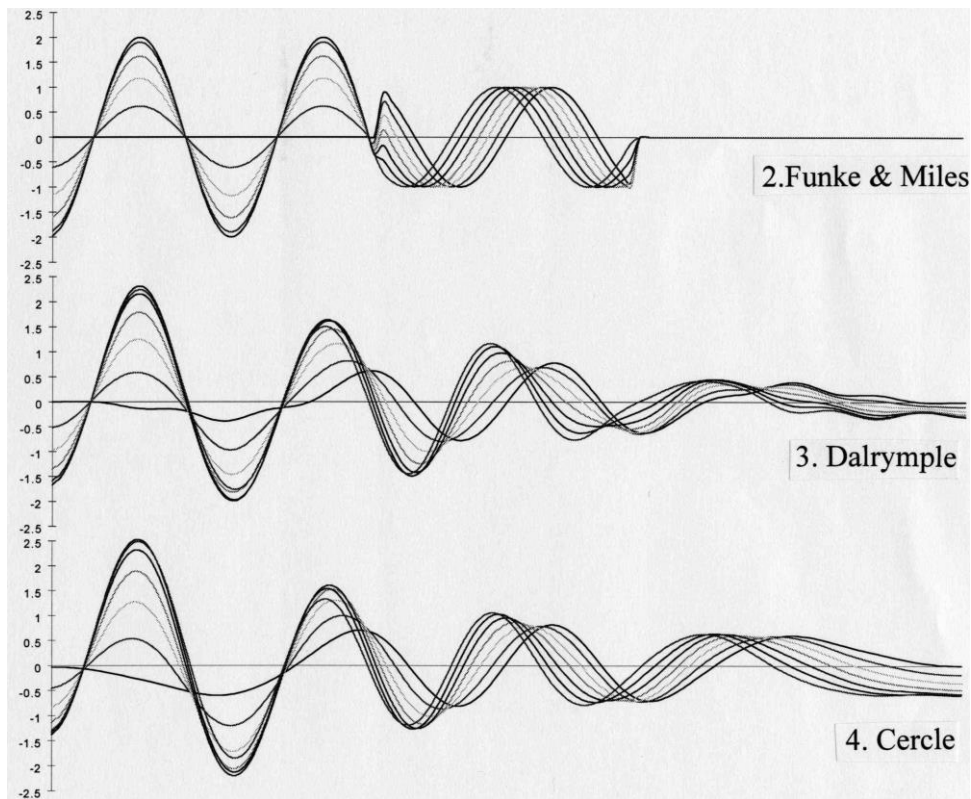
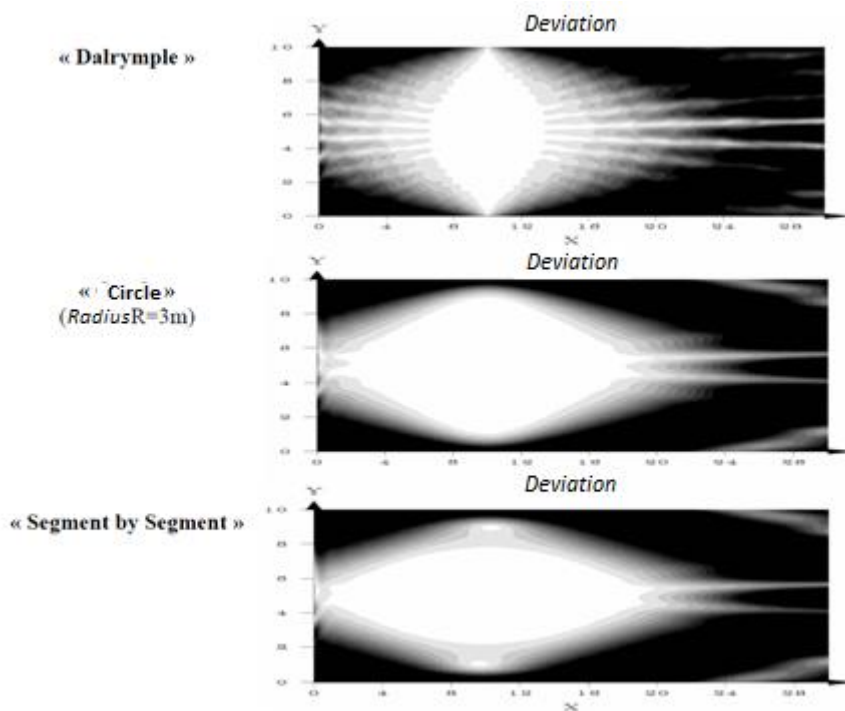


Figure 29 (Boudet and Perois 2001)

Figure 30 makes clear that the elaborated methods allow a significant improvement of the homogeneity of the wave in the target area. Besides, the circle and segment by segment methods enlarge the useful area compared to Dalrymple method.



**Figure 30 Error between generated wave fields and targets for  $T = 0.8s$ ,  $\theta = 20^\circ$ ,  $X_d = 10m$  (Boudet and Perois 2001)**

Roux de Reilhac (2008) [11] demonstrated that the disk and the rectangular methods allow to generate waves whose amplitudes are closer to the target than when Dalrymple method is used. Furthermore, the size of the useful area is well respected with both Dalrymple and disk methods, with an error on the wave amplitude of 6% for the disk method and 12% for Dalrymple on the useful areas.

### *Irregular wave*

Figure 31 and 32 present the experimental and the target spectra for the Snake's principle and the disk method. The Disk method provides a significant improvement compared to the Snake's principle in the way that the generated wave field is much more in accordance with the target wave field.

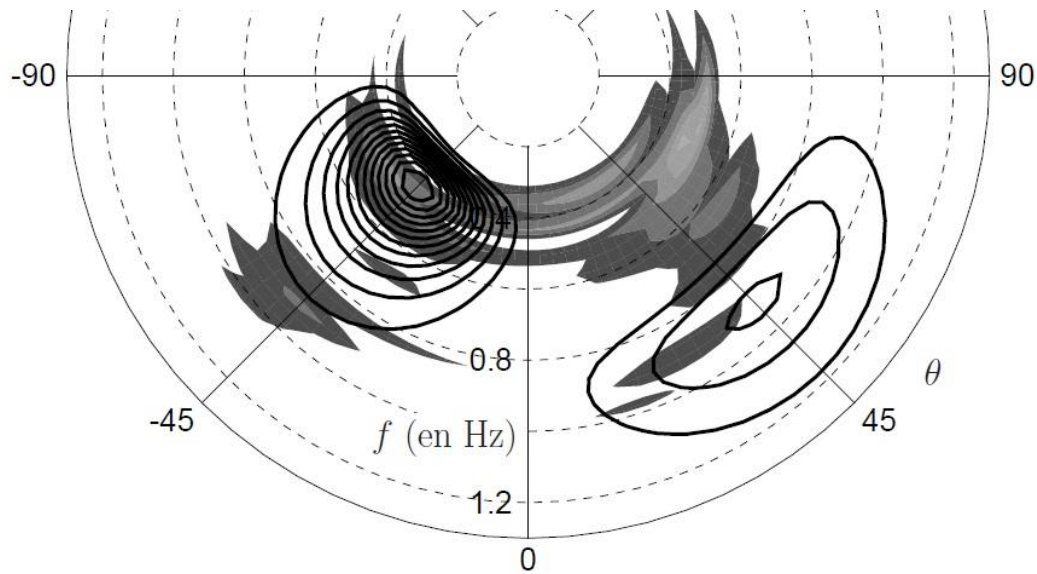


**Figure 31 Directional spectrum  $S(f, \theta)$  generated by the Snake's principle, target in solid line and experimental in greyscale (Roux de Reilhac 2008)**

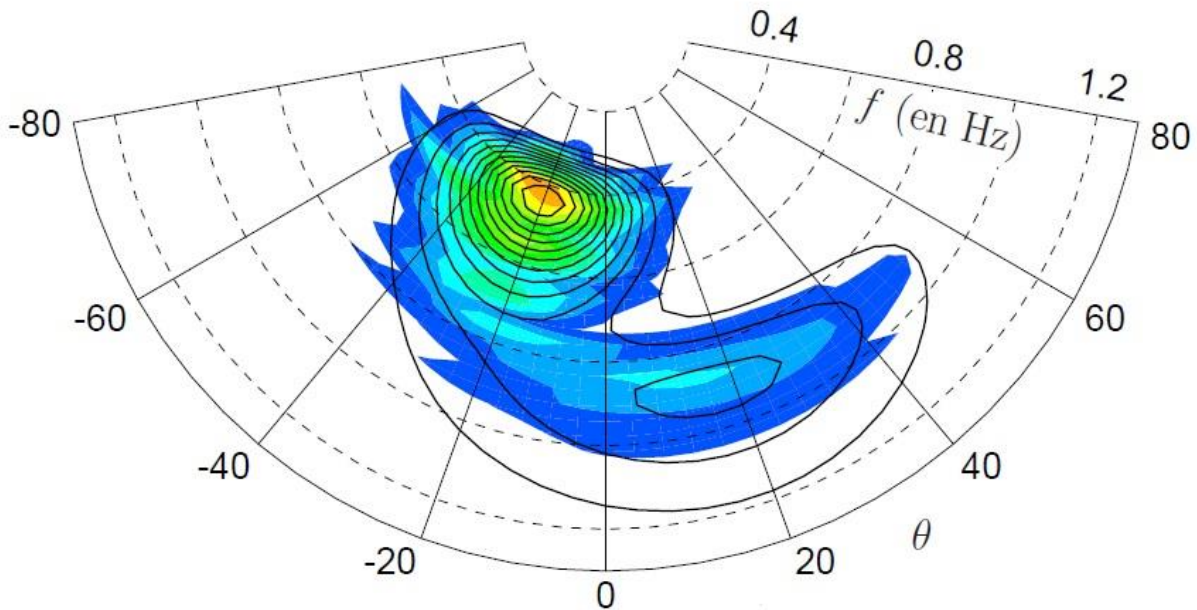


**Figure 32** Directional spectrum for the Disk Method with  $40^\circ$  between the two peaks (Ochi-Hubble modified,  $F_p^{swell} = 0.43\text{Hz}$ ,  $F_p^{wd\ sea} = 0.90\text{Hz}$  and  $s^{swell} = 18$ ,  $s^{wd\ sea} = 11$ ), (Roux de Reilhac 2008)

At the second-order, high amplitudes of spurious free waves appear outside of the target area (until more than three times the target wave amplitude!). They can lead to wave breaking or even overtopping of the basin over the side walls.

The elaborated methods allow a more accurate generation of an arbitrary wave field than the Biésel or Funke & Miles methods. Indeed, they allow getting a larger useful area and a higher homogeneity of the generated waves. Naturally, the disk and the rectangular methods are chosen depending on the experimental test to carry out. For instance, the rectangular method will be preferred to test a system with a forward speed (ex. a ship), as it allows a long dimension in the longitudinal direction (or transversal). The disk method will be used to test a fixed system.

Moreover, the disk and rectangular areas can generate better the highly directional waves.



## 5.3 GENERATION OF AN ARBITRARY WAVE-FIELD IN AN ARBITRARY BASIN (AMOEBAs)

### 5.3.1 AMOEBA wave generation principle

The *Advanced Multiple Organized Experimental Basin (AMOEBAs)* (Naito and al. (1990), (1998)) [17], [22], [23], [24], is a circular basin type composed of several wave makers called *Element-absorbing Wave maker (EAW)*. An *EAW* consists of a floating body, a voice coil motor (VCM) (Mori and Naito (1990)) and a displacement probe.

This system is designed to both generate and absorb waves simultaneously when adding the wavemaking force to the absorbing force.

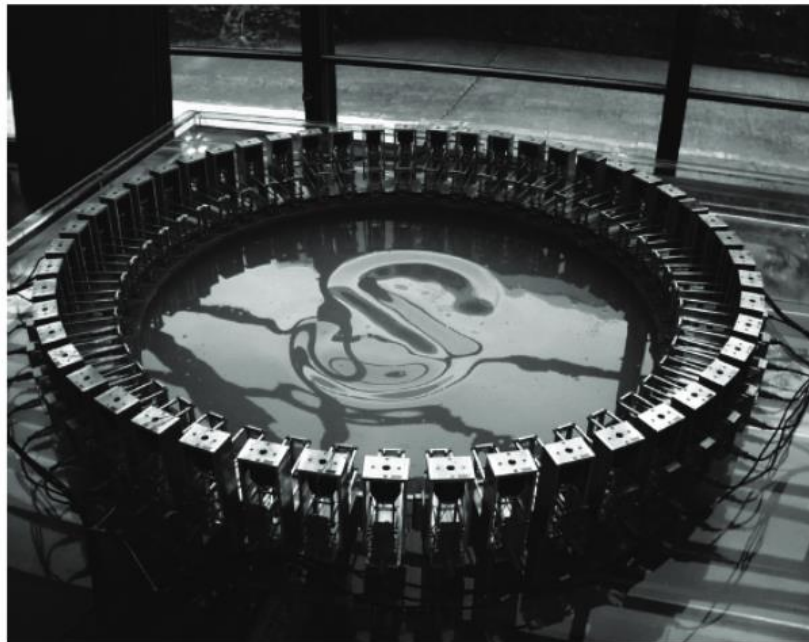


Figure 33 Photography of AMOEBA (NAOE Osaka, Japan)

An *EAW* can be expressed mathematically as a periodical wave source placed on a water surface represented by the  $0^{\text{th}}$ -order Hankel function of the first kind. Besides, an arbitrarily wave field can be described as a superposition of

Bessel functions with the Fourier-Bessel series expansion. Moreover, according to the addition theorem, a Bessel function with the origin at the centre of a circle can be described by a superposition of Hankel functions whose origins are located on the circumference of a circle. The orthogonality of the Fourier function gives the reverse relationship, expressing the Hankel function with the origins on the circumference of a circle in terms of a superposition of the Bessel functions whose origins lie at the centre of a circle. Moreover, as the Hankel function is the representation of a ring wave generated by an *EAW*, the motion of each paddle required to generate an arbitrary wave field may be known (Minoura and al. (2011)) [16].

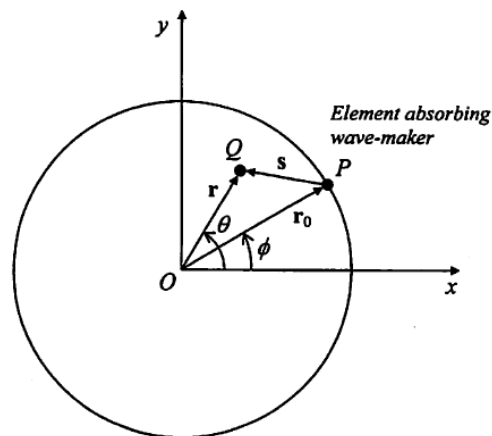
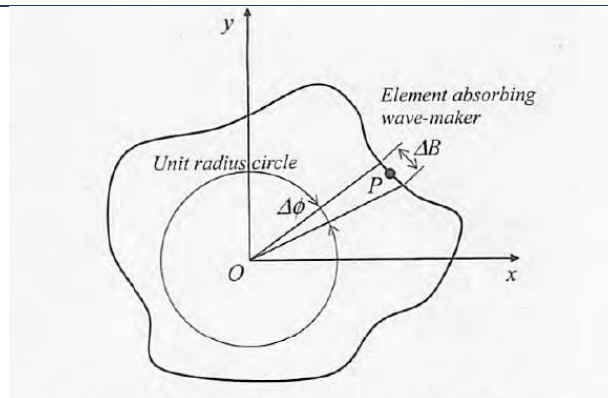


Figure34 Coordinate system for a circular basin (Minoura and Naito 2011)

### 5.3.2 Arbitrarily configured basin

The Fourier functions for a circular basin satisfy the property of orthogonality. However, this property cannot be applied for elliptic or square basins because the distance between the centre and the side walls of the basin is not constant with respect to the geometrical argument. Thereby, asymptotic expansion<sup>4</sup> of the Hankel function for large arguments is used and the orthogonality of the Fourier function is then verified.

<sup>4</sup> More details on asymptotic expansion are available in [8].



**Figure 35** Projection of wave maker breadth on unit radius circle (Minoura and Naito 2011)

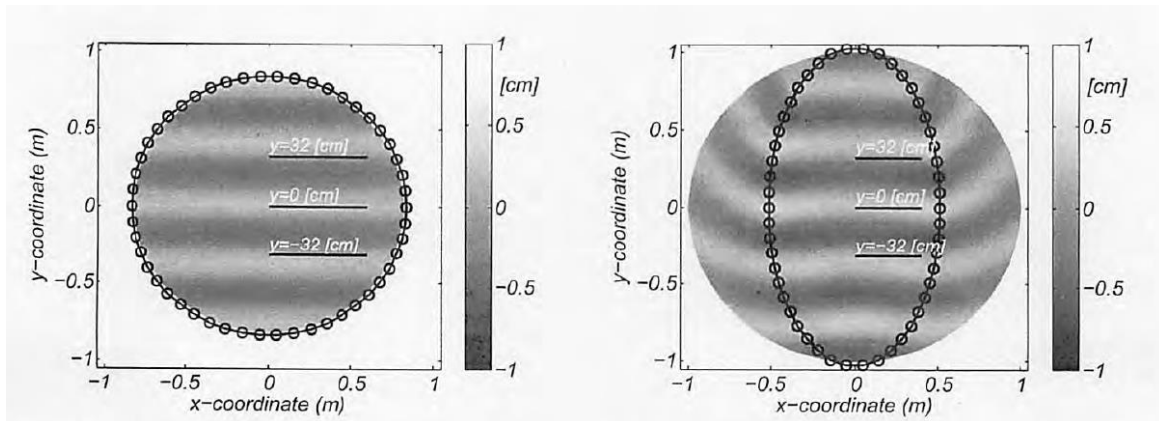


**Figure 36** Numerical calculations of regular waves generated by *EAW* in circular basin (left) and in elliptical basin (right). Circle mark = *EAW* (Minoura and Naito 2011).

This theory doesn't take into account the evanescent waves that are created close to the *EAW*. Therefore, this mathematical model provides a theory to generate long-crested regular wave field at a distance of more than at least a wavelength from the wave maker.

Numerical results show that in the case of the circular AMOEBA, the wave crest line is straight and its height is constant (figure 36: left). In contrast, for the elliptical AMOEBA the waves are bent (figure 36: right).

### Control of amplitude and phase for all EAWs

The  $i$ th and the  $j$ th wave makers are related by a phase difference that depends on the  $i - j$  distance and the wavenumber  $k$ . Besides, the amplitude of the generated waves depends on the wave direction relative to the normal of the wave maker.  $\cos\theta_j$  is the ratio of the velocity amplitude of the  $j$ th EAW to that of the direction of the wave propagation (see figure 37). Then, the wave-generating forces of the  $i$ th and  $j$ th EAW can be calculated using the phase difference between the two EAWs and the velocity amplitude  $\cos\theta_j$  (figure 87) [8].

Finally, controlling the phase of EAW's motion, one can generate transient waves at an arbitrary position of the AMOEBA.

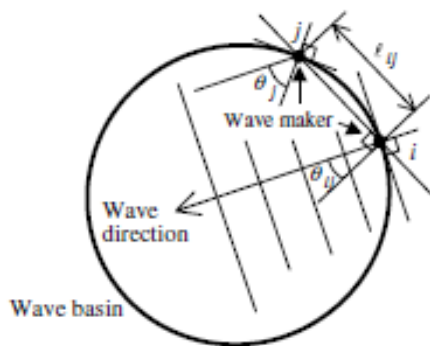


Figure 37 Wave maker synchronization

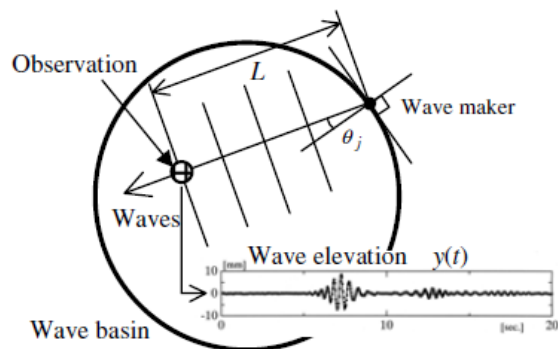


Figure 38 Wave-field for transient waves

(Naito 2006)

## 5.4 LIMITATIONS IN WAVE GENERATION

### 5.4.1 Evanescent waves

It has been seen in section 4.2.1 that evanescent waves were created due to a mismatch between the vertical geometry  $g_v(z)$  of the wave maker and the velocity profile of the generated wave. Some work has been made to find a profile of the wave maker that creates no evanescent waves (Naito and Minoura, 1994; Falnes 2002; Maguire and Ingram, 2011).

The amplitude of the evanescent waves can be quantified theoretically. Indeed, once the coefficients  $a_{0n}$  are determined with the elaborated method, the amplitudes of the evanescent modes  $a_{mn}$  can be obtained using the transfer function  $TF_{mn}$  defined as  $TF_{mn} = \frac{a_{mn}}{a_{0n}}$ .

### 2D influence

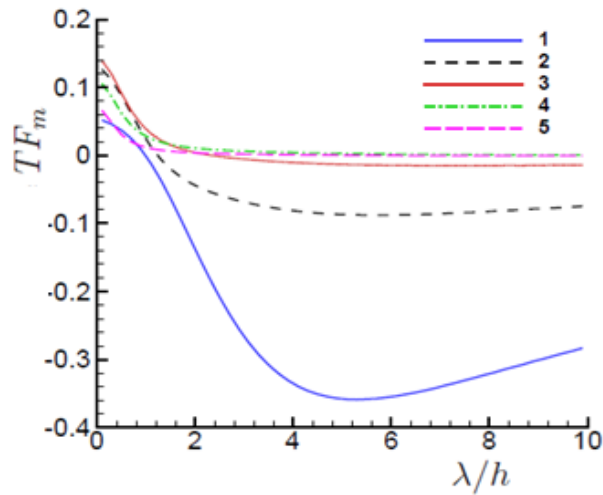
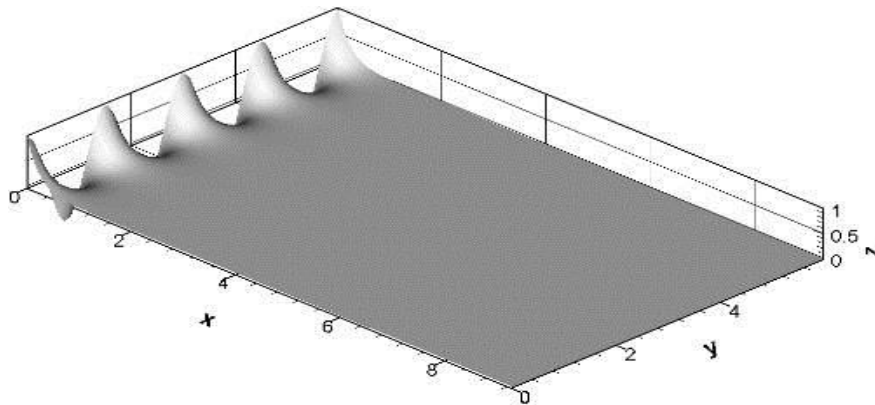


Figure 39 Contribution of the first four evanescent modes and influence of the wavelength. (Roux de Reilhac 2008)

As shown on figure 39, the two first evanescent modes have a significant contribution and become globally more important as the wavelength increases, until a maximum reached here for  $\frac{\lambda}{h} = 5$ .

---

 3D influence


**Figure 40** Evanescent waves without resonance (Bonnetfoy 2005).

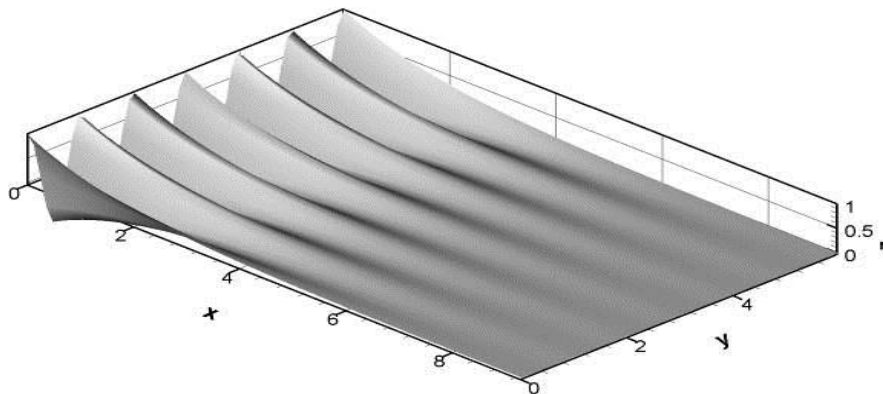


**Figure 41** Evanescent waves with resonance (Bonnetfoy 2005).

Figure 41 shows evanescent waves in the  $y$ -direction, with the presence of nodes and antinodes. For a frequency close to the basin natural frequencies, the decay along the  $x$ -direction can be slower than usual (resonance phenomenon) as illustrated on figure 42. When the generation of waves stops, the evanescent waves are transformed into quasi-standing waves oscillating in the transverse direction of the basin at one of its natural frequencies. Moreover, if there are no absorbing beaches or absorbing wave makers on the sides of the basin, the only dissipation of these evanescent waves is made through viscosity losses on the side walls. Practically, the consequence is that the basin can be disturbed during a long time. These frequencies are to be avoided during testing.

## 5.4.2 Free waves

Free waves come from the boundary condition of the velocity potential on the wave maker, at second order. The expression of the condition contains second order terms but also a forcing term made of products of first order terms. This forcing term means that even when the wave maker has a first order displacement, spurious second order waves appear and perturb the first order waves. These spurious waves are called free waves. The other second order waves are commonly called bound waves, or Stokes waves.

Let us note  $\omega^2 = k \tanh k$  the dispersion relationship of the linear waves (first order). The free wave number  $k_2^{(f)}$  is the root of the free wave's dispersion relationship  $4\omega^2 = k_2^{(f)} \tanh k_2^{(f)}$ .

In the case of an infinite depth, the free wave's pulsation is twice the first order pulsation  $\omega_2^{(f)} = 2\omega$  and the wavelength about a quarter of the first order wavelength  $\lambda_2^{(f)} = \frac{\lambda}{4}$ . Thus, the phase velocity of the free waves is equal to the half of the phase velocity:  $V_\phi^{(f)} = \frac{\omega_2^{(f)}}{k_2^{(f)}} = \frac{2\omega}{4k_1} = \frac{V_\phi}{2}$ .

### 5.4.2.1 Influence of the wavelength

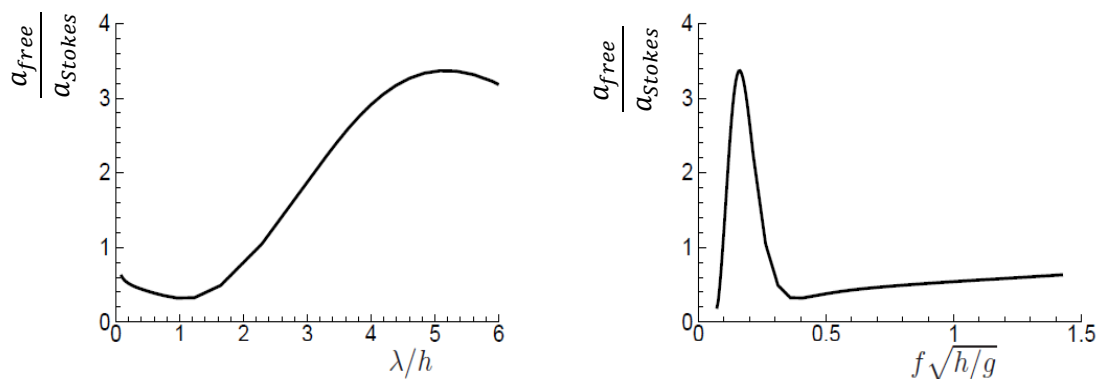


**Figure 42 Evolution of the free wave quotient in 2D in ECN wave tank (Bonnefoy 2005).**

The quotient between the free wave amplitude and the Stokes wave amplitude varies from approximately 0.5 for small wavelength  $\frac{\lambda}{h} < 2$  and increases for large wavelengths, reaching a maximum value of 3 for  $\frac{\lambda}{h} = 5$ .

### 5.4.2.2 Influence of the wave direction

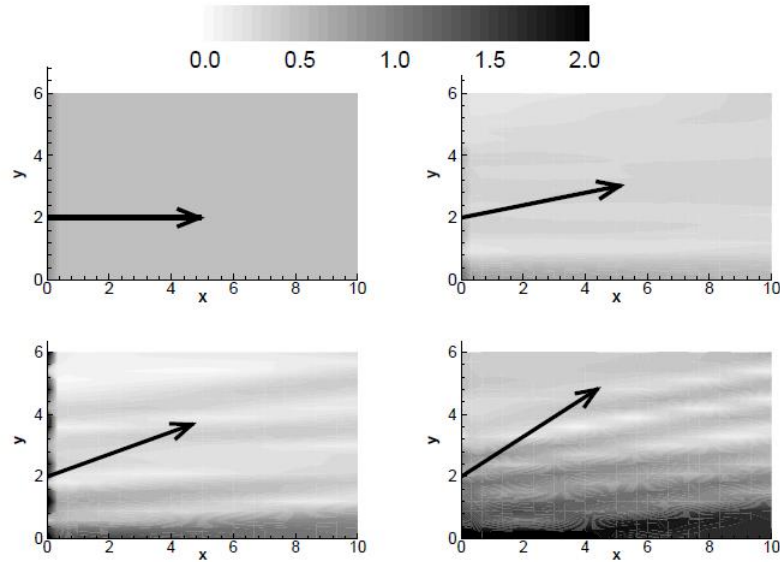


**Figure 43 Influence of the direction of propagation on the free wave amplitude for  $f=0.4\text{Hz}$  and  $\theta=0^\circ, 10^\circ, 20^\circ,$  and  $30^\circ$  (Bonney 2005).**

The dark arrows indicate the direction of propagation of the regular waves. The amplitude of the free waves globally increases with the angle of propagation.



### 5.4.2.3 Influence of the wave generation method used

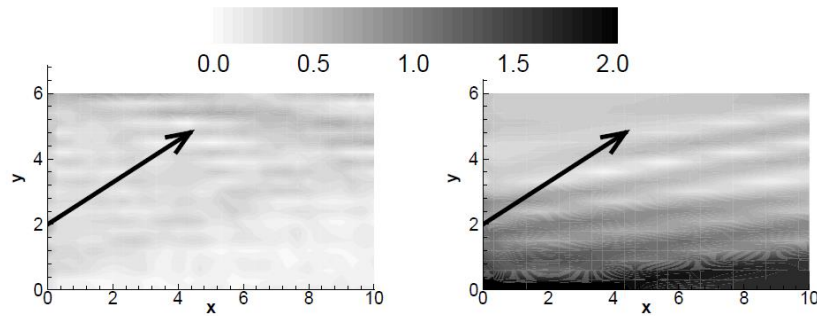


**Figure 44 Free wave amplitude for the Snake's principle (left) and Dalrymple method (right), for  $f=0.4\text{Hz}$  and  $\theta=30^\circ$  (Bonnefoy 2005).**

The level of free waves generated by the Snake's principle is lower than for the Dalrymple method. Thus, the benefits of the Dalrymple method at the first order, which allows an enlargement and a better location of the useful area, is balanced at second order by a high level of spurious free waves. For this reason, a free wave's suppression technique is needed.

### 5.4.2.4 Free waves suppression

Free waves can naturally be decomposed on the natural modes of the basin, as in section 4.2.1. Given this, the strategy to eliminate the free waves appears straightforward. The idea is to add to the wave maker's motion a second order component that generates a progressive wave train with same amplitude as that of the free waves but in phase opposition.

$$\mathbf{X}_{correction}(y, z, t) = g_v(z) \mathbf{TF}(2\omega) \mathbf{a}^{(f)}(y, t) e^{i(2\omega t + \pi)} \quad (5.19)$$

This strategy is relevant if evanescent free wave amplitude is sufficiently small. Indeed, as seen in section 4.4.1., the first evanescent mode  $n = N_1 + 1$  has a large attenuation length in the basin and significant amplitude with respect to Stokes waves. Thus, if the frequency  $2\omega$  (free wave frequency) is close to a natural transversal frequency of the basin while remaining inferior, a large attenuation length can be observed and the suppression technique becomes less effective.

### 5.4.3 Return current

In the case of second-order waves, the nonlinear effects lead to a global drift (Stokes drift) of the water particles close to the free-surface in the direction of propagation of the waves. The return current is the compensation of the Stokes drift to satisfy the mass conservation in the basin. It is represented in the wave spectrum by the zero frequency amplitude.

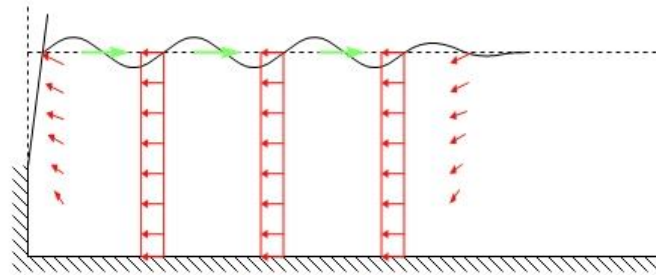


**Figure 45 Illustration of the return current in a wave tank (Bonney)**

According to the potential theory, the return current's amplitude is  $U_{return} = -\frac{\omega a^2}{2h \tanh kh}$  and its magnitude order is about 0.01m/s. Although this current is not negligible in some cases, the basin filtration can also induce a current, reducing or increasing the total current in the basin depending if it is oriented in the opposite or the same direction.

---

## 6 WAVE ABSORPTION METHODS

The fact that experimental basins are limited by solid boundaries causes wave reflections which contaminates the free-surface and then shorten the test duration. In order to conduct long and less perturbed experiments, it is interesting to use absorption mechanisms at the boundaries of the tank. Absorbers are generally classified into two types: passive and active absorption.

### 6.1 PASSIVE ABSORBERS (BEACHES)

The role of passive absorber is to damp out any wave reaching its boundary, trying to avoid the reflection of waves. Passive absorbers are usually beaches, and can be different structurally (wire screens, transversal bars,...) and geometrically (constant slope, parabolic,...). Beaches are commonly mounted in front of the wave maker, to absorb most of generated waves. However, in this configuration, the beach doesn't absorb the waves radiated, diffracted and reflected by the tested device in other directions than the beach.

Many facilities are equipped with removable foam wedges, such as University of Plymouth's wave flume and Edinburgh wave tank, whose team experimented in 1976 vertical wedge cages for beaches. For the curved tank, the beach is built using a mixture of Polyether skeleton foam and a geo-textile, Tensar. The wedges fit between two platforms of Diamond grid work staging joined together with welded steel verticals which have minimal obstruction in the dominant wave direction.

The ideal beach material would have forces that are proportional to the first power of water velocity and would ideally present the same impedance to waves as unobstructed water. Reynolds number for the smallest amplitudes and long period waves shows that we are in the viscous flow regime but the larger waves have forces which rise with velocity square. The best compromise is achieved if the beach density can be progressively increased with depth. With an increase in wedge thickness this makes the inevitable rise in impedance be gradual. (Salter, 2003)

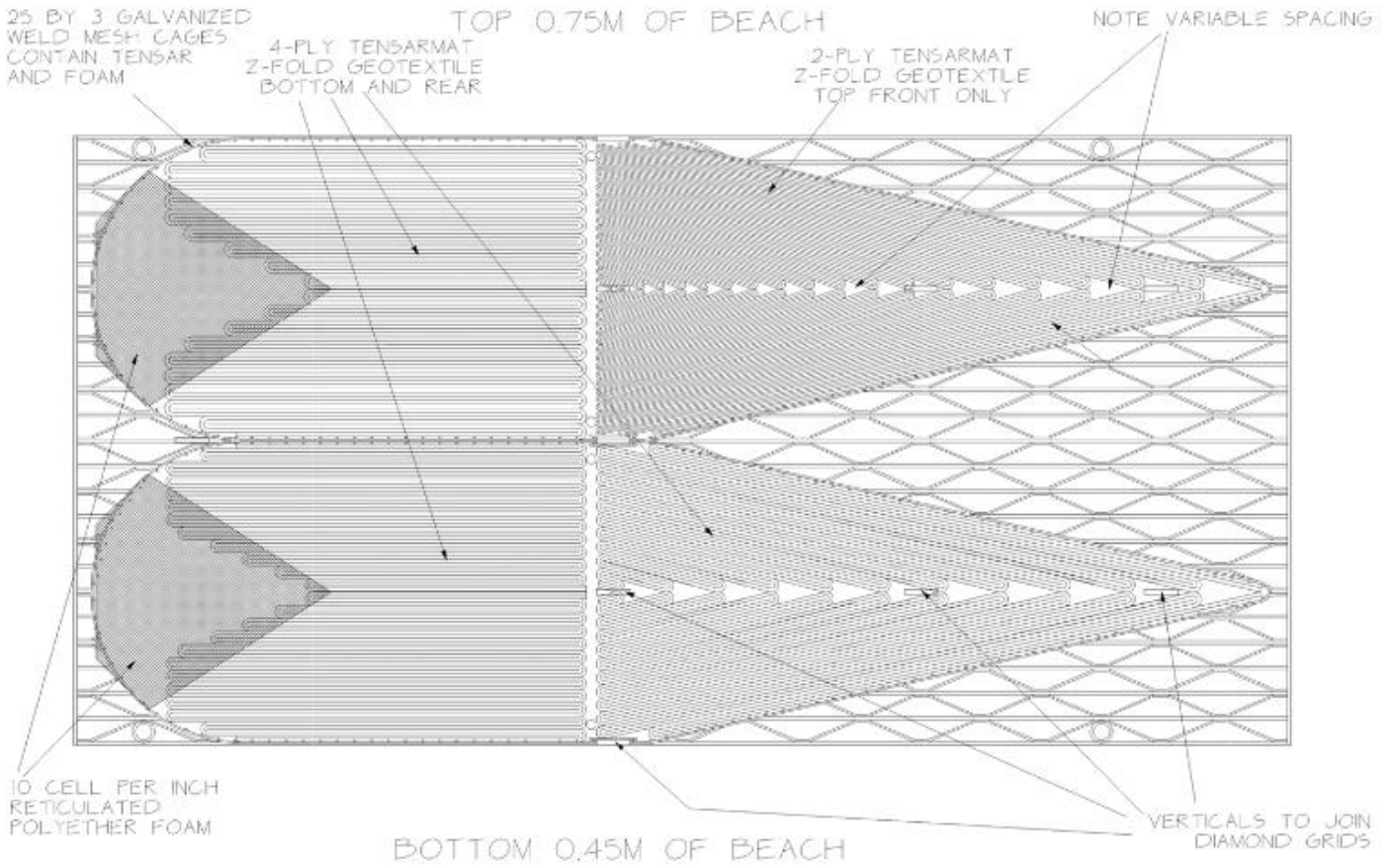


**Figure46 Packaging of the beach (UEDIN)**

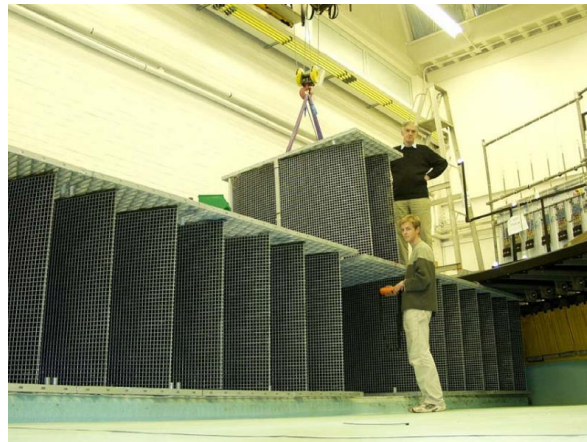


Figure 47 Picture of the beach (UEDIN)

An example of parabolic beach with convex presentation to wave fronts is shown in figure 48.



Figure 48 Ecole centrale's absorbing beach

If water is present behind the wave makers, spurious waves can be generated and passive absorber can be used behind the flaps as in the square tank of the University of São Paulo (figure 4 in section 2.1.2). The passive absorber is composed of both a beach and an absorption mesh.



Figure 49 Absorption mesh behind the flaps (University of São Paulo 2012)

## 6.2 ACTIVE ABSORBERS

### 6.2.1 Presentation.

It is essential in a finite basin to absorb the incident waves generated by the wave makers, as well as radiated and scattered waves from bodies within the basin. Hydrodynamic measurements are made and the wave maker moves in such a manner that it absorbs the incoming waves. This requires synchronizing the phases between the waves and the absorber's motion, which can be managed measuring the incoming waves and then using a feedback control system.

A first approach called 'kinematic absorption' consists in measuring the surface-elevation with gauges placed directly on the wave maker and using this information as an input for the control system (Bullock and Murton, 1989, Schäffer *et al.*, 1994; Ito *et al.*, 1996; Nohara, 1998; Liu *et al.*, 2003). Mounting the wave gauges on the wave maker has the advantage to work with a Lagrangian frame of reference, and Lagrangian dynamics is known more linear than Eulerian, allowing a broader range of validity of the linear wave theory (Woltering and Karl-Friedrich, 1994). However, as the evanescent waves are important close to the wave maker, measuring the waves on the wave maker implies taking into account the evanescent waves in the calculations which turns it to be more complicated.

As a result, another method consists in mounting the wave gauges at a certain distance from the wave maker (Milgram, 1970; Christensen and Frigaard, 1994; Frigaard and Brorsen, 1995; Nanri *et al.*, 2002). This configuration allows more calculation time to process the measurements before the waves reach the wave maker. However, this

---

anticipation has the wrong side of introducing the possibility of phase issues between the incident waves and the absorption motion (Schäffer and Klopman, 2000).

A different active absorption method called ‘dynamic absorption’ uses an input quantity (force, velocity or displacement) characterizing the absorber (and the incoming waves through the transfer function) as the input for the control system. Then, the dynamic controller provides the appropriate compensation signal (force, velocity or displacement) to generate the target wave field. Finally, the difference between an absorber and another lies in the choice of the measured quantity and the location of the measurement. According to Salter (1981), using the hydrodynamic force as feedback gives three advantages. Precision is increased as the force is an integral quantity measured over the whole wave maker front and not at a single point. There is no corrosion or dust deposit that requires frequent recalibration of the wave gauges. Finally, Salter states that force control allows knowing the energy transferred to the waves if the velocity is measured in parallel, and thus, prevent many problems due to wave’s non-linearity.

This section first gives a panel of the different absorption methods, and then presents the equation of motion of a plunger, a piston and a flap-type absorber and consequently the expression of the transfer functions between the absorber velocity and the generalized force are given. Finally, this section describes how the control system commands the absorber and a calculation of the absorption efficiency is given.

## 6.2.2 Principle and equation of motion

The fluid domain is at constant depth, with the bottom at  $z = -h$ . The side walls of the basin are assumed to be vertical, and covered by an array of  $N$  wave makers on one side of the tank. The domain is enclosed by the boundary surface  $S$  including the wave makers, the bottom of the basin, and the free surface. The normal vector  $n_i$  is directed out of the fluid domain  $S$ .

### 6.2.2.1 Principle

Maisondieu and Clément (1993) published their results on a force feedback feedforward control loop for a piston absorber. The technique uses the principle of destructive interference that can be described by the simple schemes given below in figure 49. The reflection of the incident wave on the absorber creates a reflected wave having the same frequency. If the absorber is animated with an appropriate motion, it can generate as a consequence of this motion, a radiated wave that will cancel out the reflected wave.

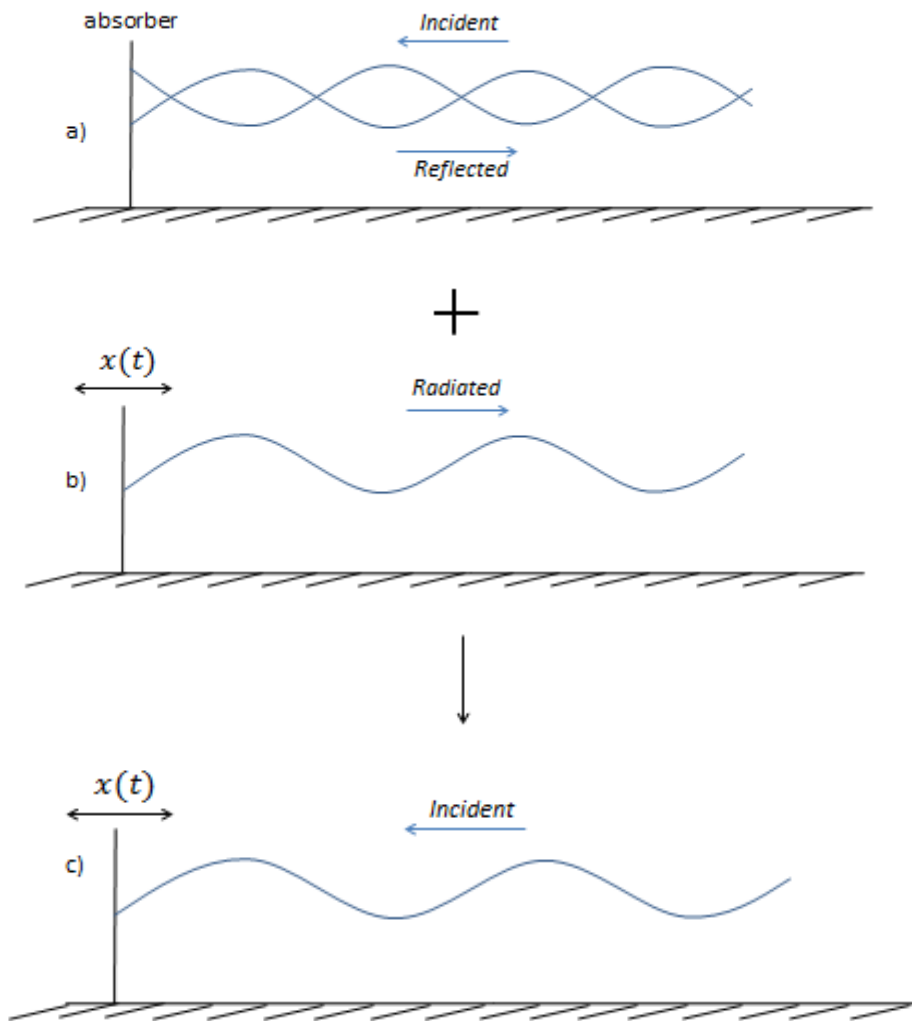


Figure 49 Illustration of the absorption principle



### 6.2.2.2 Equation of motion

#### *Equation of motion of a general type wave maker*

The  $i$ th absorber element is considered as a floating body moving with an arbitrary motion  $X$ . Thus, Newton's second law of motion gives in the frequency-domain:

$$IX''(\omega) = F_{FK} + F_D + F_R + F_H + F_C \quad (6.1)$$

where  $F_{FK}$  is the Froude-Krylov force,  $F_D$  the diffraction force,  $F_R$  the radiation force and  $F_H$  the hydrostatic force. The sum of the Froude-Krylov and the diffraction force is called the wave excitation force  $F_{ex} = F_{FK} + F_D$  and the expression of the hydrostatic force is  $F_H = -CX(\omega)$  with  $C$  the hydrostatic stiffness. Finally,  $F_C$  is the control force applied to the absorber by the motors and is composed of the absorbing force  $f_a$  and the target force  $F_t$ :  $F_C = f_a + F_t$ . The absorbing force is the force applied to the absorber in order to cancel out the reflected waves, and the target force corresponds to the force required to generate the target wave field in a basin at rest.

Concerning the generalized radiation force  $F_R$  resulting from the absorber's motion, it is defined as the unsteady radiation pressure field  $p_R(x, y, z, t)$  integrated over the  $i$ th absorber element

$$F_R = \iint_S p_R n_i dS \quad (6.2)$$

and can be expressed by the following fluid-structure formula as an instantaneous and a memory term:

$$F_R = -A(\omega = \infty)\ddot{X}(t) - \int_{-\infty}^t h(t - \tau)\ddot{X}(\tau)d\tau \quad (6.3)$$

In the frequency domain, this force may be written as the sum of an added-mass and a hydrodynamic damping term:

$$F_R = [i\omega A(\omega) + B(\omega)]\dot{X}(\omega) \quad (6.4)$$

The damping and the added-mass terms correspond respectively to the force needed to generate progressive waves and evanescent waves.

All the terms of equation (6.1) have been defined and the equation of motion of a floating body with control force  $F_C$  and submitted to a wave exciting force  $F_{ex}(\omega)$  can now be expressed in the frequency-domain as

$$F_{ex}(\omega) = \left[ (i\omega A(\omega) + B(\omega)) + i \left( \omega I - \frac{C(\omega)}{\omega} \right) \right] \dot{X}(\omega) + F_c \quad (6.5)$$

where  $A$  is the added-mass coefficient of the floating body,  $B$  the wave damping coefficient,  $I$  is the matrix of inertia and  $C$  the hydrostatic stiffness. The mechanical damping can be considered as negligible compared to both hydrodynamic damping  $B$  and added-mass coefficient  $A$  and thus, it is not taken into account in the equation above.

### *Piston-type absorber:*

In the case of a piston-type absorber, the motion is limited to translations along the x-axis and thereby, no hydrostatic stiffness term is considered. Therefore, the equation of motion of the absorber in the x direction in the frequency-domain is

$$F_{ex}(\omega) = \left[ (i\omega A(\omega) + B(\omega)) + i\omega I_{xx} \right] x'(\omega) + F_c = Z_d(\omega) V_x(\omega) + F_c \quad (6.6)$$

where  $A$ ,  $B$  and  $I_{xx}$  are expressed respectively in  $kg$ ,  $kg \cdot s^{-1}$  and  $kg$ .  $Z_d(\omega)$  is called the dynamic impedance and gives the transfer function between the horizontal velocity  $V_x(\omega)$  and the wave excitation force  $F_{ex}(\omega)$ .  $Z_d(\omega)$  will be discussed in details further.

The equation of motion can be expressed as a transfer function:

$$F_{ex}(\omega) = Z_d(\omega) V_x(\omega) + F_c \quad (6.7)$$

---

*Plunging-type absorber (AMOEBA):*



**Figure 50** Top view of some AMOEBA's absorber elements

In AMOEBA, an absorber element is seen as a floating body free to move vertically only as shown in figure 51. Thus, the arbitrary motion  $X$  becomes in this case the vertical displacement  $z$  of an absorber element.

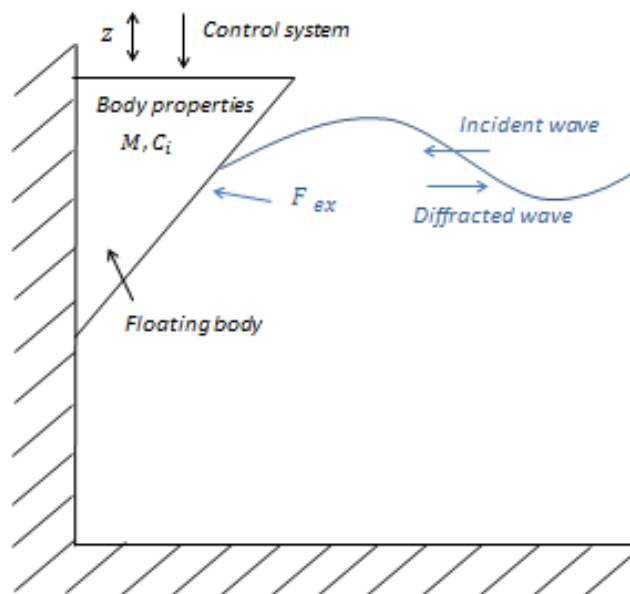


**Figure 51** Forces acting on the absorber

The equation of the vertical motion of the absorber in the frequency-domain is

$$F_{ex}(\omega) = \left[ (i\omega A(\omega) + B(\omega)) + i \left( \omega M - \frac{C(\omega)}{\omega} \right) \right] z'(\omega) + F_c = Z_d(\omega) V_z(\omega) + F_c \quad (6.8)$$

where  $A$ ,  $B$ ,  $M$  and  $C$  are expressed respectively in  $kg$ ,  $kg \cdot s^{-1}$ ,  $kg$  and  $kg \cdot s^{-2}$ .

### *Hinged-flap absorber:*

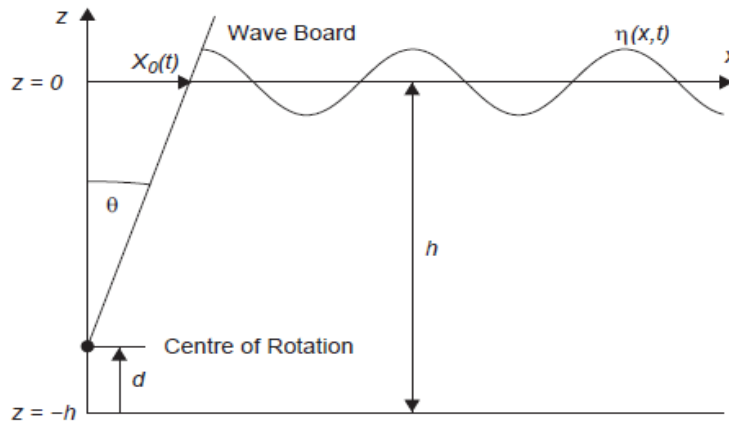


**Figure 52 Absorber geometry**

The wave maker's paddle is regarded as an inverted pendulum with the gravity-induced component varying with  $\sin\theta \approx \theta$ . Thus, the equation of motion of a flap-paddle is

$$T_{ex}(\omega) = (I_y + A(\omega)) \ddot{\theta}(\omega) + B(\omega) \dot{\theta}(\omega) - C(\omega) \theta(\omega) + T_c \quad (6.9)$$

$T_{ex}$  represents the wave excitation torque acting on the flap and is the sum of the paddle dynamic torque  $T_p$  and the radiated torque  $T_R$ , while  $T_c$  is the control torque. More details are presented in (Spinneken & Swan 2009).  $I_y$  ( $kg \cdot m^2$ ) is the moment of inertia with respect to the  $y$  axis. As the variables considered in the case of a flap-type

absorber are the torque and the angular velocity instead of the force and the velocity,  $A$ ,  $B$ ,  $I_y$  and  $C$  are respectively in  $kg.m^2$ ,  $kg.m^2.s^{-1}$ ,  $kg.m^2$  and  $kg.m^2.s^{-2}$ .

The equation of motion can be expressed as a transfer function relating the angular velocity of a flap  $\Omega(\omega)$  to the torque induced by the wave excitation forces  $T_{ex}(\omega)$ :

$$T_{ex}(\omega) = Z_d(\omega)\Omega(\omega) + T_c \quad (6.10)$$

## 6.2.3 The control system

### 6.2.3.1 Impedance approach: impedance matching

The method applied for wave absorption using force-feedback controlled machines is based on an approach comparable to impedance matching in signal transmission. Here the dynamic impedance  $Z_d$  can be decomposed into  $Z_d = R_d + iY_d$ , where  $R_d$  is the radiation resistance or commonly called hydrodynamic damping (progressive part of radiated wave energy) and  $Y_d$  the radiation reactance (evanescent part of radiated wave energy) of one absorber element (Spinneken & Swan (2009)). The dynamic impedance  $Z_d$  reflects how much a body resists to the motion when submitted to a given force. It includes both wave-induced quantities as well as the wave board dynamics as seen in (2). As a result,  $Z_d$  is dependent on the geometry of the wave maker. Naito (2006) and Falnes (2002) published a theory giving  $Z_d$  for flap and piston-type wave makers and Maguire (2011) developed a theory for cosine and hyperbolic cosine shaped paddles.

Besides, the absorption of the incident wave force is achieved integrating an external dynamic system with artificial absorption impedance  $Z_a = R_a + iY_a$ , equivalent mechanically to a damper  $b$  and a spring  $c$ . The coefficients  $b(\omega_0)$  and  $c(\omega_0)$  can't be readjusted instantaneously and for this reason, they must be optimised for a fixed frequency  $\omega_0$  and remain constant during a run. This is due to the difficulty to recalculate them instantly and at each time-step (convolution product in the time-domain). This dynamic system creates a force signal  $f_a(\omega) = Z_a(\omega)X'(\omega)$  that is added to the feedback force (force measured by the transducers). Its role in the control loop will be described further in figures 55 & 56.

### 6.2.3.2 Equation of motion with the external dynamic system

We consider the absorption of waves for an arbitrary-type absorber. The generalized absorbing force value created by the external system is

$$f_a(\omega) = b(\omega_0)X'(\omega) + c(\omega_0)X(\omega) = Z_a(\omega)X'(\omega) \quad (6.11)$$

Therefore, the general equation of motion of an absorber working with the dynamic control mechanism is:

$$F_{ex} = (M + A(\omega))X''(\omega) + (b(\omega_0) + B(\omega))X'(\omega) + (c(\omega_0) + C)X(\omega) + F_t \quad (6.12)$$

And can be written as

$$F_{ex} = \{Z_d(\omega) + Z_a(\omega)\}X'(\omega) + F_t \quad (6.13)$$

Two schemes of absorbers with their control dynamic system are given respectively in figure 53 for a plunging-type absorber and in 54 for a flap-type absorber.

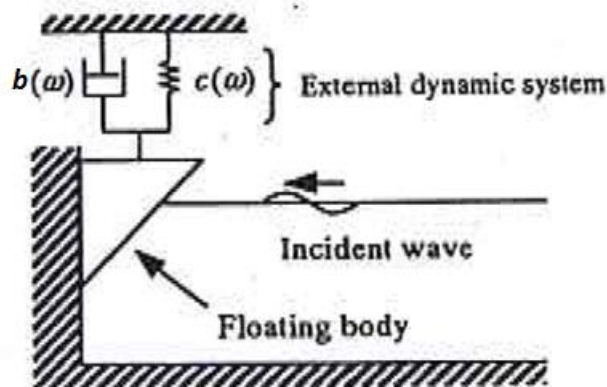


Figure 53 Dynamic system for AMOEBA

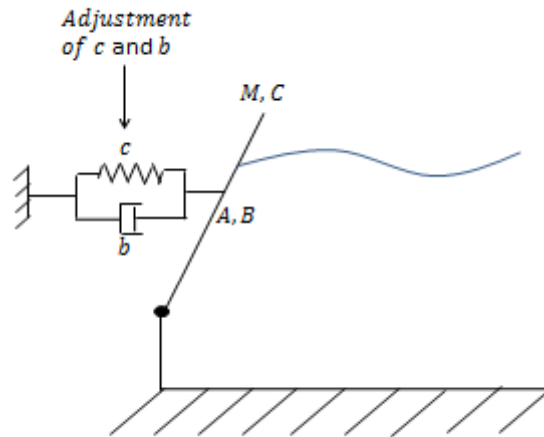


Figure 54 Dynamic system for a flap-type absorber

### 6.2.3.3 Optimum coefficients for the dynamic control

Falnes (1993) states that there are two conditions to maximize power absorption, which are working with the optimum phase and the optimum amplitude, that lead to the expression of the maximum power absorption  $Z_a = Z_a^*$ , equivalent to  $R_a = R_d$  and  $Y_a = -Y_d$ . According to (6.5) and (6.11), the expressions of the two impedances are

$$Z_d = B(\omega) + i \left( \omega(M + A(\omega)) - \frac{c(\omega)}{\omega} \right) \quad (6.14)$$

and

$$Z_a = b(\omega_0) - i \frac{c(\omega_0)}{\omega} \quad (6.15)$$

Therefore, the values of  $b$  and  $c$  that maximize the absorption efficiency (Bessho (1973)) are:

$$c(\omega_0) = \omega_0^2 \{M + A(\omega_0)\} - C(\omega_0) \quad (6.16)$$

and

$$b(\omega_0) = B(\omega_0) \quad (6.17)$$

### 6.2.3.4 The control dynamic system

The wave exciting force  $F_{ex}$  acting on the transducer is used as a feedback force as shown on 55. The difference between this force and the target force is minimized by the controller  $C_0(\omega)$  (not discussed herein) through a process referred as ‘closing the loop’. Besides, the absorption is achieved through an absorbing force  $f_a$  created by the absorbing impedance  $Z_a$ , constructed artificially with the displacement measurement of the floating body (gives  $z$  and  $z'$ ) and the values of the external dynamic system  $b(\omega_0)$  and  $c(\omega_0)$ . These later parameters are given by equation (6.16) and (6.17), once the added-mass  $A(\omega)$  and the wave damping coefficient  $B(\omega)$  calculated by Ursell-Tasai’s method as a two-dimensional problem. Experimental tests reveal that the values of  $b(\omega_0)$  and  $c(\omega_0)$  are in good agreement with the theory, excepted that  $c(\omega_0)$  is smaller in experiments than in theory and the cause is supposed to be an electric effect of the control circuit (Naito and Minoura 1999).

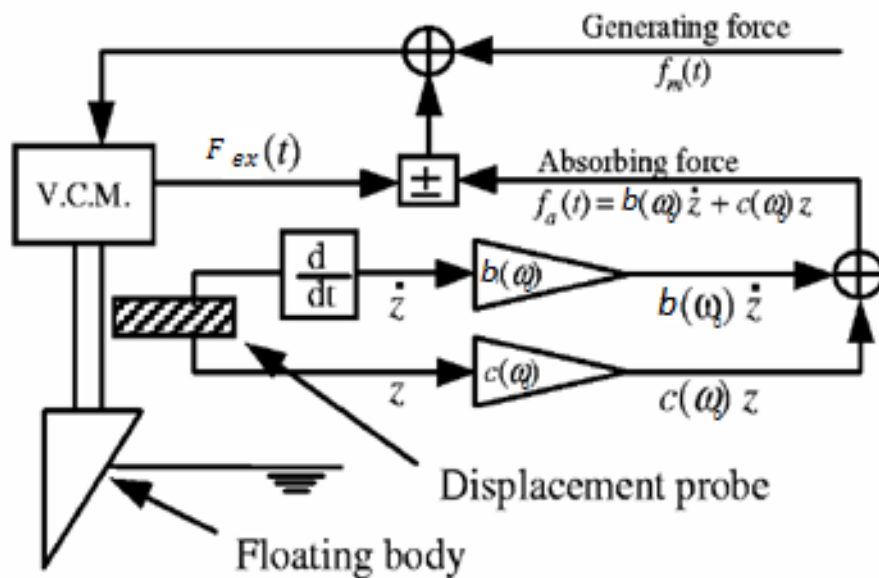


Figure 55 Wave maker element logic control diagram of AMOEBA (Naito & Alli, 1998). V.C.M stands for voice coil motor.

Figure 56 shows a block diagram of the entire wave machine control system for the case of a flap-type absorber with  $G(\omega) = \frac{\Omega(\omega)}{T(\omega)}$  the wave board dynamic function,  $Z_a(\omega)$  the absorption filter and  $Z_d(\omega) = \frac{1}{G(\omega)}$  the dynamic torque feedback. The main particularity of the system described in figure 56 compared to the one shown in figure 55 is that the feedback is made using the paddle angle instead of a force value measured by a transducer on the absorber.



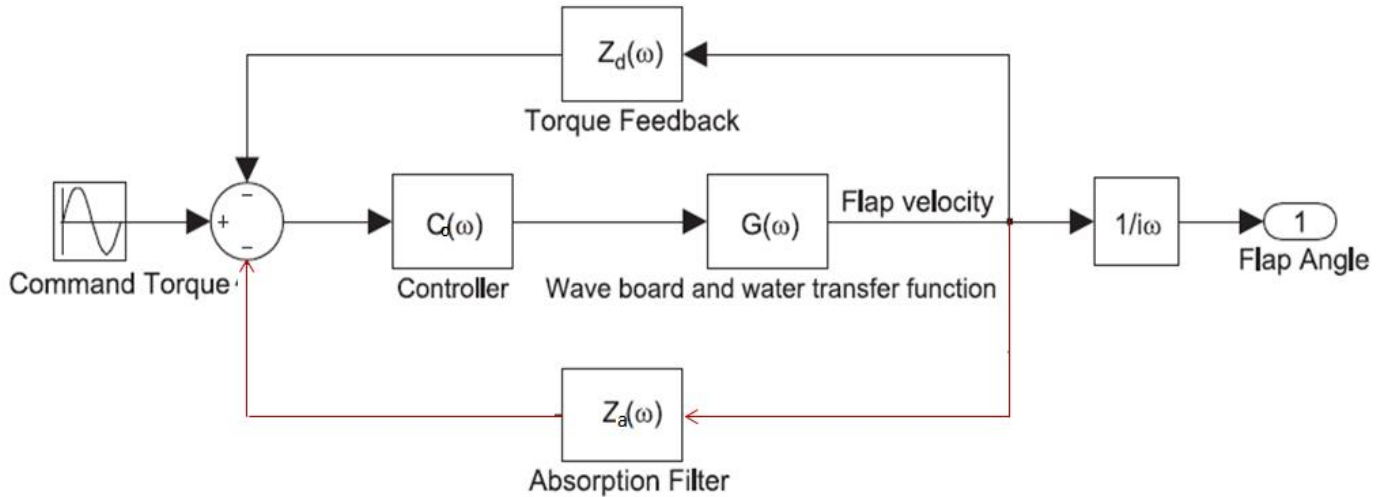


Figure 56 General system model for a flap-type absorber-wave maker (Spinneken & Swan 2009)

Obviously, all systems can generate waves while absorbing the incoming waves by adding a command signal. Applying standard frequency-domain methods, the block diagram in figure 56 may be expressed as a single transfer function

$$H(\omega) = \frac{1}{i\omega} \frac{C(\omega)G(\omega)}{1+C(\omega)G(\omega)[Z_a(\omega)+Z_d(\omega)]} \quad (6.18)$$

where  $H(\omega)$  relates the command torque to the flap angle for a matched absorption filter and closed-loop control and can now be used to model and simulate the behaviour of the wave maker/absorber.

## 6.2.4 Absorption efficiency

### 6.2.4.1 Definition

The time-averaged power of the external mechanism, which is converted from the hydrodynamic force  $F_{ex}$ , is:

$$\overline{W} = \frac{1}{2} \omega^2 b(\omega_0) |X^0|^2 \quad (6.19)$$

where  $X^0$  is the time-averaged amplitude of a wave maker element's motion.

In the case of irregular waves, the absorption efficiency is defined as

$$\eta = \frac{E_T}{E_\omega} \quad (6.20)$$

where  $E_T = \frac{1}{2\pi} \lim_{T \rightarrow \infty} \frac{1}{T} \int_{-\infty}^{\infty} Z_f(\omega) X'(\omega) d\omega$  is the absorbed power and  $E_\omega = \frac{\rho g^2}{2} \int_0^{\infty} \frac{S(\omega)}{\omega} d\omega$  is the wave spectrum energy.

However, a term is non-causal in the expression of  $E_T$  and it is possible to make it causal using the Kramers-Krönig (K-K) or Bode relations [7]. Thus, the absorption efficiency when a control force with causality is active modifies  $E_T$  into

$$\overline{E}_T = \frac{\rho g^2}{2} \int_0^{\infty} C_e(\omega) \frac{S(\omega)}{\omega} d\omega < 1 \quad (6.21)$$

where  $C_e(\omega)$  is the absorption coefficient of irregular waves and is expressed as below

$$C_e(\omega) = \frac{b^2(\omega)}{b^2(\omega) + [\omega\{A(\omega) - \{A(\infty)\}\}]^2} \quad (6.22)$$

and the power of the spectrum  $S(\omega)$  is perfectly absorbed when  $C_e(\omega) = 1$ .

It has been seen that it is required to choose a fixed frequency to calculate the external coefficients  $b$  and  $c$ . For irregular waves, the chosen frequency must coincide with the peak frequency  $\omega_0$  of the irregular waves spectrum to enhance the absorption. As a result, the absorption coefficient is called "constant coefficient system" (Naito 2006) and becomes

$$C_{ec}(\omega) = \frac{4\omega^2 B(\omega) b(\omega_0)}{\omega^2 \{B(\omega) + b(\omega_0)\}^2 + \{(\omega_0^2 - \omega^2)M + \omega_0^2 A(\omega_0) - \omega^2 A(\omega)\}^2} \quad (6.23)$$

### 6.2.4.2 Quality of the absorption

#### Experimental results

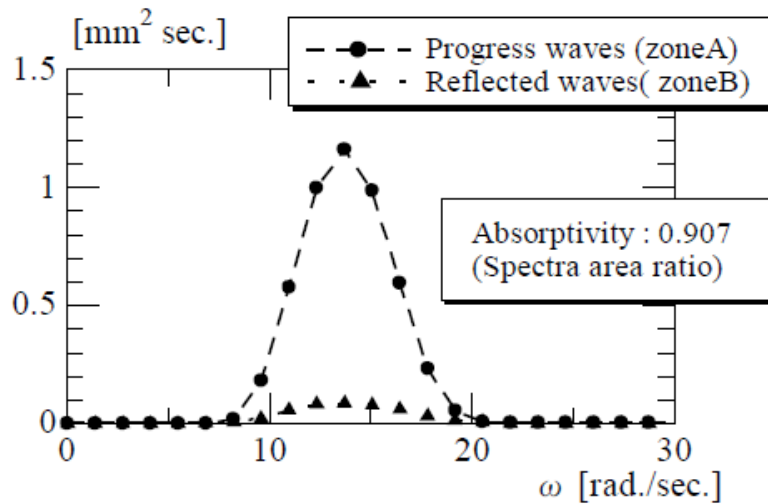


Figure 57 Power spectra of transient waves measured experimentally (Naito & Minoura 1999).

Figure 57 shows that even if some components of irregular waves are not absorbed, until 90.7% of the energy spectrum can nonetheless be extracted from the incoming waves.

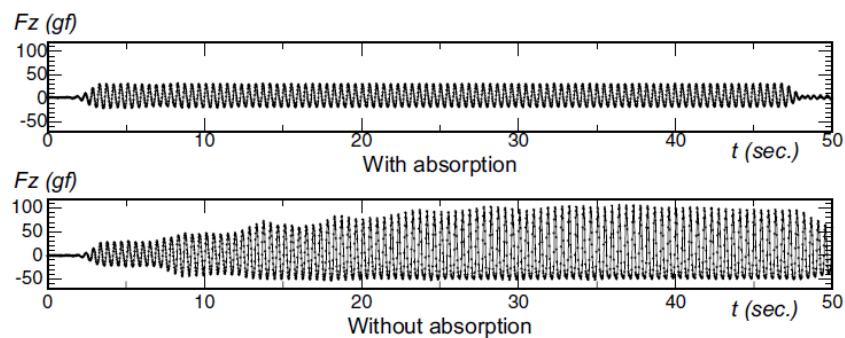
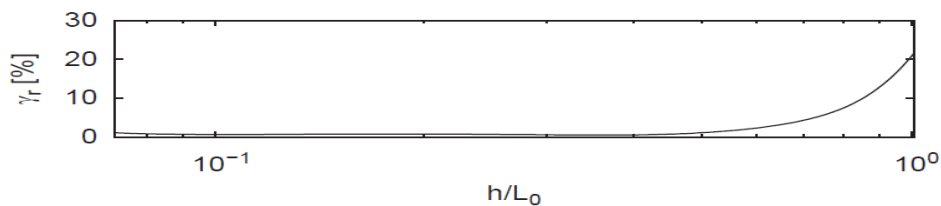


Figure 58 Comparison of measured time series data, for a circular wave basin (AMOEBA), of wave-exciting heave force acting on a sphere model in regular waves with and without absorption. (Naito 2006)

A visual example of dynamic absorption efficiency is given on figure 58. It demonstrates the possibility of conducting long duration experiments with either regular waves or irregular waves with a narrow-banded spectrum, as almost all incoming waves are absorbed by the absorbers elements.

### *Quality over the range of frequency*

The filter impedance does not match exactly to the complex conjugate dynamic impedance  $Z_d^*$  over the full frequency range. Figure 59 shows the value of the reflection coefficient defined by Falnes (2002). The absorption becomes poor when the filter fails to match the machine's reactance  $Y_d$ , and this happens for high frequency waves. This limitation is caused by the inertia of the absorber that avoids high frequency motions. Nonetheless, very good power absorption is achieved over a wide band of interest **for regular waves**.



**Figure 59 Power reflection coefficient  $\gamma_r$  over the range of wavelength (Spinneken & Swann 2009).**

According to Naito (1999), the optimal parameters of the external dynamic system are adjusted for one regular wave and must be readjusted for another regular wave. Thereby, a mismatch appears in the case of irregular waves between the filter impedance and the radiation impedance for some components of the spectrum and as a result, reflected waves remain.

### Quality in terms of wave direction

Contrary to the absorption of uni-directional waves, it is difficult to develop a matching approach for the absorption of multidirectional waves. Indeed,  $A(\omega)$  and  $B(\omega)$  are dependent on the angle of incidence  $\beta$ . The dependence of  $A$  on  $\beta$  is shown on figure 60 whilst  $B$  is simply proportional to  $\frac{1}{\cos\beta}$ .

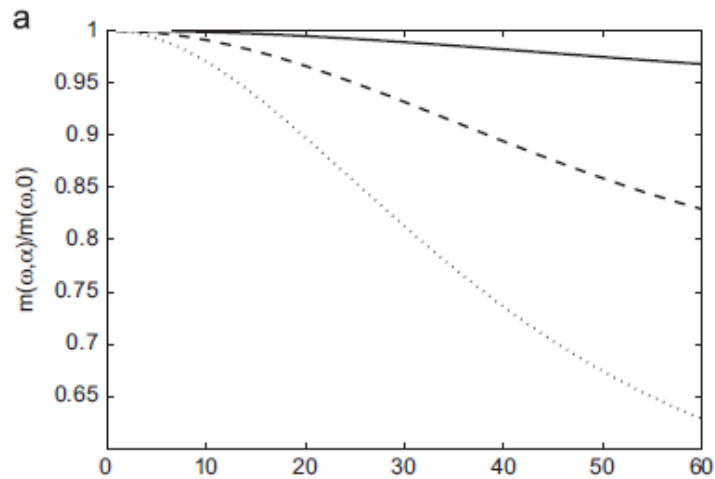


**Figure 60 Added-mass coefficient normalized by the two-dimensional added-mass (for  $\beta = 0^\circ$ ) for three different wavelengths: \_\_\_  $h/L_0 = 0.1$ , ---  $h/L_0 = 0.3$ , .....  $h/L_0 = 0.5$ . (Spinneken & Swann 2012)**

Given this angular dependency, the ideal absorption controller would need to adjust the parameters  $a(\omega)$  and  $b(\omega)$ . Nevertheless, Spinneken & Swann (2012) considered a controller which is optimized for a 2D case and used it for 3D absorption. The results are shown on figure 61 and appear acceptable. Note that  $\delta = 1$  corresponds to perfect absorption.

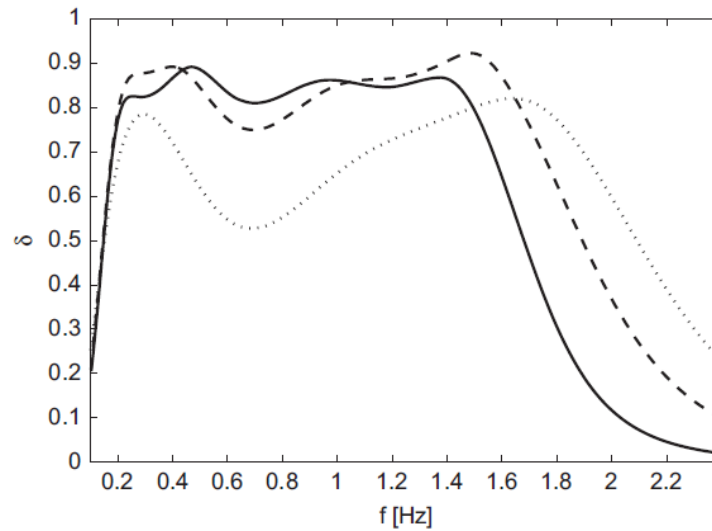


**Figure 61 Amplitude absorption coefficient for a flap-type wave maker ( $d/h=0.533$  ;  $h=1.5m$ ), the controller being optimised for  $\alpha = 0$ : —  $\alpha = 0^\circ$ , - -  $\alpha = 30^\circ$ , ...  $\alpha = 60^\circ$ . (Spinneken & Swann 2012)**

Schäffer and Skourup (1996) described the theory of a multidirectional wave absorber based on the differentiation of the wave elevations measured on each absorber. This information is in principle sufficient to know the wave direction. The method was tested numerically and the results shown on figure 62 demonstrate the interest of 3D absorption as the coefficient of absorption is significantly reduced when an active 3D absorption is used instead of a 2D absorption.

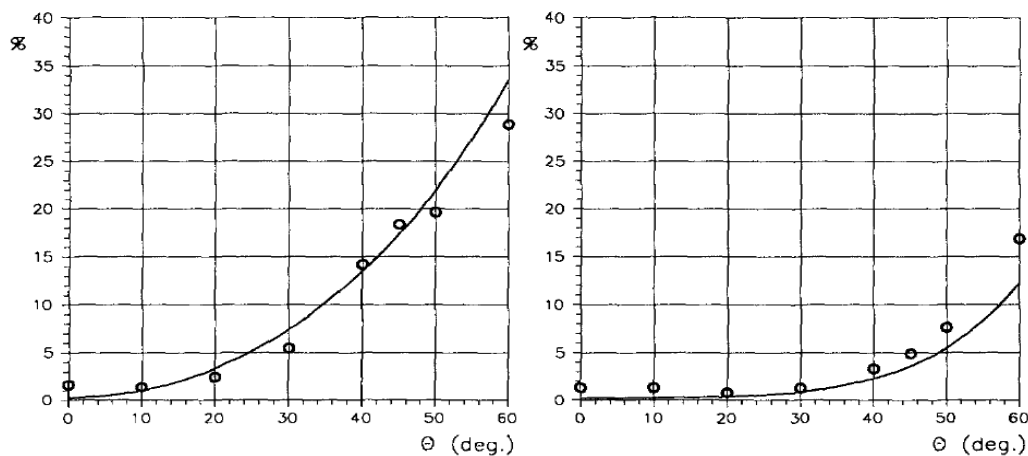


**Figure 62 Reflection coefficients (%) for regular waves of frequency 0.4Hz versus angle of attack for 2D-AWACS (left) and 3D-AWACS (right). The full curves give the theoretical performance (Schäffer & Skourup 1996).**

## 6.2.5 Frequency adaptation.

Chatry & Clément (1998) developed an absorption technique that measures the force on the absorber with transducers. The measurements are used as input values for the velocity control loop (see velocity feedforward in figure 63).

The Self-adaptative Feedforward-Feedback (SAFF) controller (figure 63) calculates an estimation of the 'instantaneous incident wave frequency' through the Extended Kalman Frequency Estimator and integrates its value in the control loop, computing the transfer functions  $P(\omega)$  and  $H^*(\omega)$  at the instantaneous pulsation  $\omega$ . Therefore, the piston's motion is optimized for the incoming waves and the absorption efficiency is enhanced as shown on figure 64.

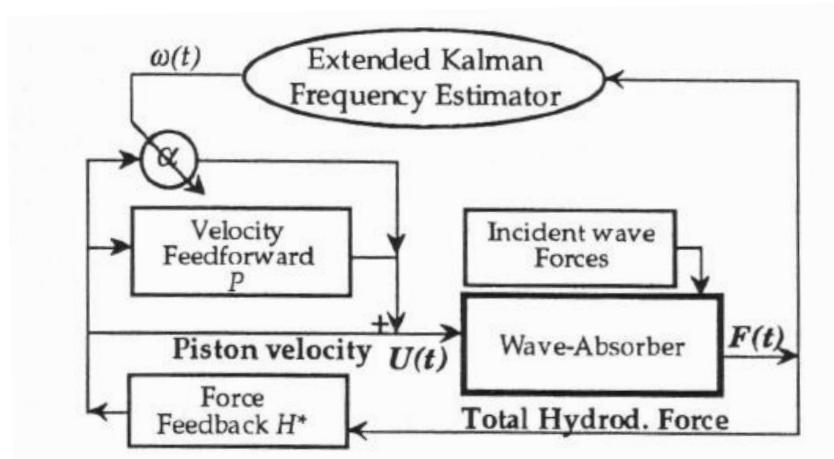
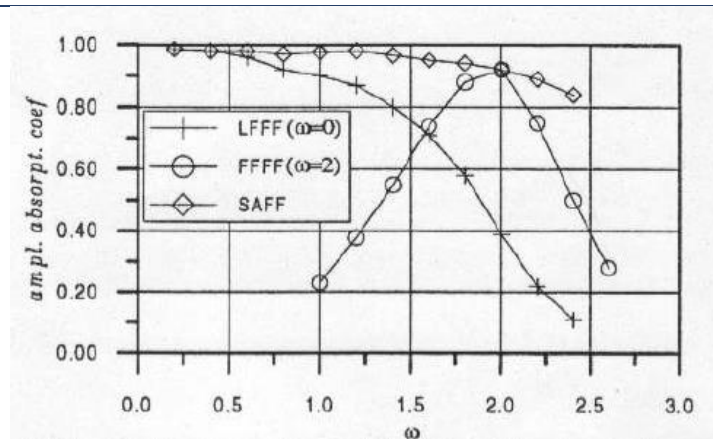


Figure 63 Self-adaptative Feedforward-Feedback (SAFF) controller. Block diagram (C. Maisondieu, A. Clément ISOPE 1998)



**Figure 64 Absorption coefficient for the three proposed absorber control types (C. Maisondieu, A. Clement ISOPE 1998)**

The *Low Frequency Feedback-Feedforward* (LFFF) and the *Fixed Frequency Feedback-Feedforward* (FFFF) whose corresponding absorption coefficient are plotted in figure 54 refer to controllers that are optimized respectively for  $\omega = 0 \text{ rad/s}$  and for a fixed pulsation  $\omega = \omega_0$  (here  $\omega_0 = 2 \text{ rad/s}$ ).

### CONCLUSION ON ACTIVE ABSORPTION

Dynamic absorption is nowadays the most effective technique for wave absorption, followed by kinematic absorption and beaches. However, one of its weak points is that the optimum coefficients of the control system are optimized for one regular wave (one frequency and one direction of propagation) and can't be changed in time. Therefore, this method does not enable a perfect absorption of irregular waves. Moreover, the absorber has difficulties to absorb high-frequency waves due to the absorber's inertia. Besides, the directional consideration (3-D absorption) is a real issue and few absorbers take it into account.

Thus, optimal absorption can be achieved in most of the facilities at only one frequency in the spectrum and for one direction of wave. Dynamic absorption still has to be improved, especially to efficiently absorb broad-banded short-crested waves.



---

## 7 SHALLOW WATER ASPECTS FOR MARINE ENERGY DEVICES

Most types of wave tanks are set up with a fixed water depth. This is an issue for WECs as it does not always ensure the compliance of the wave kinematics between the model and the real scale. A solution is therefore to adjust the water depth in the tank, and this can be made possible either by adjusting the water level in the tank or by using an adjustable test-bed that can be set anywhere. As a result, the wave maker must also be set at the corresponding height. The piston-type does not require any adjustment and the plunging-type can easily be adjusted because it is constructed to move vertically. Concerning the flap-type wave maker, the modification is more complex because the whole wave maker system (paddles & motors) must be set at the right height.

In addition to the wave kinematics similarity, the moorings similarity must also be satisfied. First of all, in order to satisfy the mooring length compliance, a grid of thread connection points can be put on the bottom of the tank to connect the moorings at a higher depth than the tank depth. It does not perturb the wave kinematics as much as large concrete blocks might induce. Then, different technologies and materials can be used to create the scaled moorings, in order to reflect the correct hydrodynamic properties (stiffness and damping).

However, even with these devices, the shallow water basin must be sufficiently wide to ensure reproducibility in term of moorings length, especially for catenary moorings. Finally, basins with a sloping bottom may be relevant to test WECs, in order to better reproduce a possible change in bathymetry.

---

## 8 CONCLUSION

The generation of realistic sea states at scale model in basins of finite dimension is being improved step by step, the tanks limits being relentlessly pushed back. Accurate complex wave fields can be generated in arbitrary basins. Even current and wind (not presented herein) can be generated simultaneously with wave, providing more resemblance with the real sea conditions. In addition to that, some basins are dedicated to particular aspects such as shallow water, coastal engineering (sediments) ...

Concerning wave absorption, there are still some progress to be made, particularly in terms of frequency adaptation and angular dependency of the control system. However nowadays, one is able to carry out experiments during a long time because of the small level of spurious waves such as reflected waves, free waves, radiated and diffracted waves from the tested system.

---

## 9 REFERENCES

### References for the types of wave makers:

- [1] Hughes, S. A., 1993, Physical models and laboratory techniques in coastal engineering.
- [2] Equimar - Assessment of current practice for tank testing of small marine energy converters.  
<https://www.wiki.ed.ac.uk/download/attachments/9142387/D3.3.pdf?version=1>
- [3] J. Alcino de Andrade Martins, Comments on the wave field of circular tank, University of São Paulo.
- [4] Shih, R., Chou, C., 2009, Numerical modelling of 3D oblique waves by L-type Multiple directional wave generator.
- [5] Hiraishi, T., Hirayama, K., 1998. Generation of double peak directional wave by Dual Mode Snake-type wave maker.
- [6] Mello, P.C., Carneiro, M.L., 2011. A control and automation system for wave basins.
- [7] Salter S.H., (1981). Absorbing wave-makers and wide tanks, Proceedings. Directional Wave Spectra Applications, Berkeley, Am.Soc.Civ.Eng, p185-202
- [8] J.R.M Taylor, M. Rea, D.J. Rogers, (2003). The Edinburgh curved tank. School of Engineering and Electronics, University of Edinburgh. 5<sup>th</sup> EWTEC. Cork, Ireland.
- [9] S., Uto, K., Maeda, (2008). Deep Sea Basin at National Research Institute of Japan.
- [10] S.H.S. Salter, (2003). "Relocation of a Multidirectional Mixed Wave Spectrum Test-Tank with Modifications for Reduced Area and Minimum Cross-wave Errors", Final EPSRC report, Grant GR/R64438/01.
- [11] T.Davey, I.Bryden, D.M. Ingram, A.Robinson, J.L. Sinfield and A.R. Wallace. The All-Waters Test Facility- a new resource for the marine energy sector. 4<sup>th</sup> International conference on Ocean Energy, ICOE 2012, Dublin.



---

[12] Hiraishi, T., 2002. Wave transformation in multi-face current generation basin.

**References for Random wave simulation:**

[13] Frigaard, P., 1993. Wave generation theory.

[14] Payne, G., 2008. Guidance for the experimental tank testing of wave energy converters.

[15] Chakrabarti, S.K. , 1994. Offshore structure modeling.

**References for wave generation methods:**

[16] Bonnefoy, F., thèse de doctorat, 2005, Modélisation expérimentale et numérique des états de mer complexes.

[17] Minoura, M., 2011, Generation of arbitrary wave field in an arbitrarily configured wave basin composed of element-absorbing wave makers. International Journal of Offshore and Polar Engineering (ISSN 1053-5381).

[18] Bonnefoy, F., Le Touzé, D., Ferrant, P., 2003, Second order directional wave maker theory : prediction and control of free waves.

[19] Shaver M.D., 1989, Regular wave conditions in a directional wave basin. Master thesis.

[20] Roux de Reilhac, P., 2008, thèse de doctorat, Génération de houle multidirectionnelle en bassin d'essais, influence de la directionnalité de la houle sur les mouvements d'un navire.

[21] Boudet, L., Perois, J.P., 2001, Nouvelles techniques de pilotage d'un batteur segmenté pour la génération de houle oblique.

---

**References for active absorption:**

- [22] Naito, S., 2006. Wave generation and absorption in wave basins: theory and applications. *International Journal of Offshore and Polar Engineering* 16 (2), 81–89.
- [23] Martins, 2006. Wave and force measurements in circular compact basin.
- [24] Naito, S., 1999. Evaluation of Performance of New-wave making Basin.
- [25] Masterton, S., Swan, C., 2008. On the accurate and efficient calibration of a 3d wave basin. *Ocean Engineering* 35 (8–9), 763–773.
- [26] Spinneken, J., Swan, C., 2009, Second-order wave maker theory using force-feedback control. Part I. A new theory for regular wave generation. *Ocean Engineering*, in press, doi:10.1016/j.oceaneng.2009.01.019.
- [27] Spinneken, J., Swan, 2009, Second-order wave maker theory using force-feedback control. Part II: An experimental verification of regular wave generation.
- [28] Spinneken, J., Swan, 2012, The operation of a 3D wave basin in force control.
- [29] Newman, J. N., 2008, Analysis of wave generators and absorbers in basins.
- [30] Maisondieu, C., Clement, A., A realizable force feedback-feedforward control loop for a piston wave absorber.
- [31] Maisondieu, C., 1993, thèse de doctorat, L'absorption dynamique des ondes de gravité en régime instationnaire.
- [32] Maguire, E. A., 2011, PhD thesis, Hydrodynamics, control and numerical modeling of absorbing wave makers.
- [33] Salter, S.H., 1981, Absorbing wave-makers and wide tanks.